國立臺灣大學工學院環境工程學研究所

碩士論文

Graduate Institute of Environmental Engineering

College of Engineering

National Taiwan University

Master Thesis

# 以鈀銅奈米團簇配合電化學方法選擇性還原生成氨氮與氮氣之研究

# Electrochemical nitrate reduction using palladium-copper nanoclusters toward $N_2$ and $NH_3$ selectivity

鄭明勳

Myeong-Hoon Jeong

指導教授： 林逸彬 博士

Advisor: Yi-Pin Lin, Ph.D.

中華民國 112 年 7 月

July 2023

doi:10.6342/NTU202303029

# 國立臺灣大學碩士學位論文
# 口試委員會審定書
## MASTER'S THESIS ACCEPTANCE CERTIFICATE
## NATIONAL TAIWAN UNIVERSITY

Electrochemical nitrate reduction using palladium-copper nanoclusters toward $N_2$ and $NH_3$ selectivity

本論文係 鄭明勳 R10541137 在國立臺灣大學環境工程學研究所完成之碩士學位論文，於民國 112 年 7 月 28 日 承下列考試委員審查通過及口試及格，特此證明。

論文審查委員 Oral examination committee:

林逸彬 博士
國立臺灣大學環境工程學研究所教授

席行正 博士
國立臺灣大學環境工程學研究所教授

潘述元 博士
國立臺灣大學生物及環境系統工程學系助理教授

指導老師 Advisor

系主任/所長 Director



doi:10.6342/NTU202303029

# Acknowledgments

Already two years have passed, and I have reached the culmination of my master's degree. I am truly grateful to all those who have helped me during these two years. As I complete my thesis, I want to thank those who have supported me.

First and foremost, I am thankful to Professor Lin, who provided me with guidance and encouragement more passionately than anyone else. In the beginning, with my limited English and presentation skills, you encouraged and advised me without reproaching, and for that, I am truly grateful. You always treated me as a researcher, guiding me by asking questions about my mistakes rather than reprimanding them, and I am truly thankful for that.

卓儀秦, in the beginning, when I didn't know much about the topic of my thesis and how to use NOVA, you taught me many things with a smile, even your busy schedule. Especially, you helped me figure out how to use the XRD and XPS machines and how to communicate with them, making it much easier for me. To my laboratory friends 余佳洪, 白文豪, 紀煜騰, 許聖翔, there are so many things I am grateful for that it's hard to write them all down. Firstly, 佳洪, thank you for buying reagents for me in your busy schedule. 文豪, thank you for discussing the theoretical aspects and providing many experimental suggestions. 煜騰, thank you for always helping with the experimental setups and other



doi:10.6342/NTU202303029

troublesome tasks. 聖翔, thank you for speaking to me in Korean with a smiling face. Having a reliable friend like you made me feel truly thankful.

To our international students, thank you so much for the past two years. You guys greeted me with a smile during class, provided support and encouragement when I was tired, filled in the gaps I had, and even took the time to watch rehearsals and give feedback despite your busy schedules. I am truly grateful.

For this entire process in Taiwan, I want to express my deepest gratitude to our parents, who provided me with these opportunities, encouragement, and courage.



doi:10.6342/NTU202303029

# Abstract

This study investigated Cu monometallic and PdCu bimetallic electrodes prepared on Ni foam with varying plating times for the reduction of nitrate. SEM images revealed the morphology evolution, with Cu/Ni electrodes exhibiting agglomerated granules transforming into rhombus structures as plating time increased. Increasing plating time led to a higher Cu proportion, an increased Cu(200)/Cu(111) ratio, and larger crystallite sizes for Cu(111) and Cu(200). PdCu/Ni showed a grape-cluster-like surface with accumulated palladium particles on the surface of copper. Electrochemical impedance spectroscopy indicated the improved electron transfer for the Cu/Ni electrodes and the additional plating of Pd showed an even better electron transfer. The double-layer capacitance ($C_{dl}$) revealed that the surface area activity increased with extended plating time for Cu from 2.6 to 5.5$mF/cm^2$. Nitrate reduction experiments on Cu monometallic electrode demonstrated high removal efficiency and achieving 100% nitrate removal at 210 minutes, with $NH_4^+$ as the main product. Bimetallic electrode; PdCu10min/Ni exhibited enhanced activity than Cu monometallic electrode. Under constant potential, $NO_3^-$ was fully converted to $NH_4^+$ without $N_2$ generation in acidic condition. PdCu bimetallic electrode showed consistent performance over multiple cycles but no $N_2$ was generated. Electrochlorination with the addition of $Cl^-$ enhanced nitrogen gas evolution and resulted in a low ammonia residual.



doi:10.6342/NTU202303029

**Keywords: Electrochemical nitrate reduction, Copper, Palladium, Electrochlorination**



doi:10.6342/NTU202303029

# Table of Content





doi:10.6342/NTU202303029

doi:10.6342/NTU202303029

# List of Figures





doi:10.6342/NTU202303029

doi:10.6342/NTU202303029

doi:10.6342/NTU202303029

# List of Tables





doi:10.6342/NTU202303029

# Chapter 1 Introduction

## 1.1. Background

Nitric acid is an important industrial chemical that is used in the production of a wide range of products, such as fertilizers, explosives, and dyes (Speight., 2017). However, discharge of wastewater containing nitric acid can cause negative environmental impacts, mainly due to the presence of nitrate and its reduction product nitrite. Human activities, including the application of fertilizers, the release of industrial and domestic effluents, and emissions from combustion engines, have the potential to contribute to the excessive release of nitrate and nitrite into the environment. These can cause adverse health effects in humans and the environment (Fewtrell et al., 2004; Hornung et al., 1999; Njock et al, 2023). Hence, Taiwan Environmental Protection Administration (Taiwan EPA) have limited 10 mg N/L $NO_3^-$ and 0.1 mg N/L $NO_2^-$ for drinking water quality standards in Taiwan (Taiwan EPA, 2022).

Considering the potential health and environmental risks associated with excessive levels of nitrate and nitrite, electrochemical reduction using an effective metallic or bimetallic electrode reveals a promising approach to remove nitrate and nitrite (Min et al., 2021). However, there is limited research exploring the effect of crystal morphology of



doi:10.6342/NTU202303029

the electrode on the selectivity of reduction end products between $N_2$ and $NH_3$ under acidic conditions, which could be encountered in industrial effluents containing nitric acid. This study aims to fill the knowledge gap by investigating the nitrate reduction using copper (Cu) and palladium - copper (PdCu) electrodes.

## 1.2. Research objective

The objectives of this study are:

1. To investigate the nitrate reduction performance by different Cu electrodes with different Cu(200)/Cu(111) facet ratios under acidic conditions.

2. To evaluate the performance of PdCu bimetallic electrode for nitrate reduction.

3. To study reusability of electrode.

4. To study the influence of $Cl^-$ on the nitrogen gas evolution during of nitrate reduction.



doi:10.6342/NTU202303029

# Chapter 2 Literature review

## 2.1. The presence of nitrate and nitrite in the environments

Nitric acid ($HNO_3$) has been used as a versatile chemical with various applications for centuries. The notable property of nitric acid is its capability to effectively eliminate undesired surface deposits from a wide range of materials, including metals, glass, and ceramics. (SSINA, 2022). Additionally, it is used to make the production of explosives, such as nitrobenzene derivatives, dinitrotoluene derivatives, and TNT derivatives (Speight, J. G., 2017). Nitric acid is also commonly utilized for etching various metals, purifying gold and silver, and manufacturing of fertilizers and synthetic dyes (Hocking, M. B., 2005).

Even though nitric acid is a useful chemical in various industries, its use can also result in environmental impacts, particularly when it is used in large quantities or in ways that lead to its release into the environment (Manisalidis et al., 2020). Furthermore, when nitric acid is released into water, it can form nitrates with other chemicals and compounds. Nitrate is frequently found as a pollutant in both surface and groundwater and can contribute to eutrophication and harm aquatic ecosystems. In addition to the direct release of nitric acid into waterways, nitrates can also form from the breakdown of other nitrogen-containing compounds, such as fertilizers and animal waste (Moloantoa et al., 2022).



doi:10.6342/NTU202303029

## 2.2. Traditional nitrate, nitrite treatments

Nitrate and nitrite can undergo treatment through a range of technologies, including reverse osmosis, ion exchange, and biological denitrification. Reverse osmosis is more appropriate for smaller-scale treatments (Shelly et al., 2021), whereas ion exchange is frequently used for large-scale ones (Kurt et al., 2012). However, both processes generate waste streams containing concentrated nitrate and nitrite that require additional treatment prior to disposal. Biological denitrification process, which uses microorganisms to convert nitrate and nitrite into nitrogen gas, has much potential. However, it is susceptible to pH fluctuations and the presence of additional salts (Zhang et al., 2023).

## 2.3. Electrochemical Nitrate Reduction

Electrochemical nitrate reduction to $NH_3$ or $N_2$ has gained significant research attention due to its various benefits. Firstly, it can offer a highly efficient method to reduce nitrate levels in water to meet regulatory requirements. Secondly, unlike conventional treatment methods, electrochemical nitrate reduction can minimize the use of additional chemicals and formation of byproducts, resulting in a more cost effective and environmentally friendly approach. Finally, the compatibility of electrochemical nitrate reduction with existing water treatment infrastructure makes it a promising solution for



doi:10.6342/NTU202303029

treating nitrate contaminated water. The production of nitrogen gas by electrochemical nitrate reduction is harmless. In some cases, the ammonia converted from nitrate can be used for fertilizer production or energy transportation (Giddey et al., 2017).

To achieve efficient nitrate removal, electrode property plays an important role. Numerous metals have been investigated for electrochemical nitrate reduction, including transition metals such as Fe, Cu, Sn, Ni and noble metals such as Pd, Pt, Ru (Teng et al., 2022). For transition metals, Cu has exhibited the greatest nitrate reduction to nitrite performance among those transition metals, which is the rate-limiting step of the entire pathway from $NO_3^-$ to $N_2$ and $NH_3$. While, for noble metals, they can combine atomic hydrogen ($H\cdot$) as a strong reducing agent for $NO_3^-$ reduction (Duca et al., 2012). However, single noble metal, such as, Pd, Pt does not efficiently convert $NO_3^-$ to $NO_2^-$. Even though single noble metal possesses a low removal rate of nitrate, they can maintain the stability of the electrocatalyst by combining a secondary transition metal such as Cu, Sn, and In, which is defined as the bimetallic catalyst.

Bimetallic catalyst has been demonstrated to be a more efficient catalyst for nitrate reduction than monometallic catalyst because bimetallic catalyst is H-affinity metal which can form high binding energy of $H_{ads}$ and significantly enhance the indirect $NO_3^-$ reduction through hydrogenation (Wang et al., 2021).



doi:10.6342/NTU202303029

For example, Wu et al. reported that by plating different amounts of Pd nanocluster to Sn on a Ni form to form $Pd_xSn_{100-x}$/Ni electrodes, a high selective $N_2$ (79%) formation can be achieved at $Pd_5Sn_{95}$/Ni. On the other hand, the monometallic catalyst Sn on the Ni form only achieved a low selectivity of $N_2$ (52%) (Wu et al., 2022). Cerrón-Calle et al. researched the selective nitrate reduction using Cu-Pt foam and reported that the bimetallic catalyst Cu-Pt160s presented 94% nitrate conversion compared to 55% nitrate conversion obtained using monometallic Cu catalyst in 120 min (Cerrón-Calle et al., 2022). Li et al. reported that $Cu_{80}Pb_{20}$, $Cu_{80}Pd_{20}$, and $Cu_{80}Ni_{20}$ bimetallic electrodes achieved high nitrogen gas selectivity compared to Cu monometallic electrode (Li et al., 2018).

The formation of $NH_3$ or $N_2$ as the final products of $NO_3^-$ reduction could also depend on the crystal facet (Shin et al., 2020, Wu et al., 2022), applying potential (Shen et al., 2020), pH value (Zhang et al., 2018), the ratio between H-affinity metal and O-affinity metal (Favarini et al., 2020), and the supporting matrix (Li, J et al., 2021). For instance, Su et al. (2020) prepared Sn electrodes using different metal deposition sequences, electrical charges, and metal compositions and found that a higher yield of $N_2$ could be achieved for Sn (420) compared to other crystal facets ((214), (131), (420)) of Sn due to its optimal arrangement of active sites for bond breaking after nitrate



doi:10.6342/NTU202303029

adsorption (Su et al., 2020). Shin et al. (2020) prepared Cu electrodes with different Cu(200)/Cu(111) crystal facet ratios by using surfactants, such as cetyltrimethylammonium chloride (CTAB), polydiallyldimethylammonium chloride (PDDA), and benzethonium chloride (BZT) and different electrodeposition times and they found that a higher area ratio of Cu (111) enhanced the formation of $N_2$ at pH 8.5.

### 2.4. Mechanism of Nitrate reduction on Metallic catalyst

Understanding the mechanism of electrochemical nitrate reduction is crucial. Multiple electrons and protons are transferred during this procedure. Below reactions are commonly exhibited for the production of $N_2$ and $NH_3$ from the electrochemical reduction of $NO_3^-$ (Cao et al., 2023).

$$2NO_3^- + 12H^+ + 10e^- \rightarrow N_2 + 6H_2O, E^0 = 1.17V \text{ vs SHE} \quad (1)$$

$$NO_3^- + 9H^+ + 8e^+ \rightarrow NH_3 + 3H_2O, E^0 = -0.12V \text{ vs SHE} \quad (2)$$



doi:10.6342/NTU202303029

As shown in Figure 1, several byproducts could be generated including nitrite $NO_2^-$, hydroxylamine $NH_2OH$, and nitrous oxide $N_2O$ (Garcia-Segura et al., 2018). However, these byproducts are thermodynamically unstable and easily convert to $N_2$ and $NH_3$ (Ai et al., 2022).

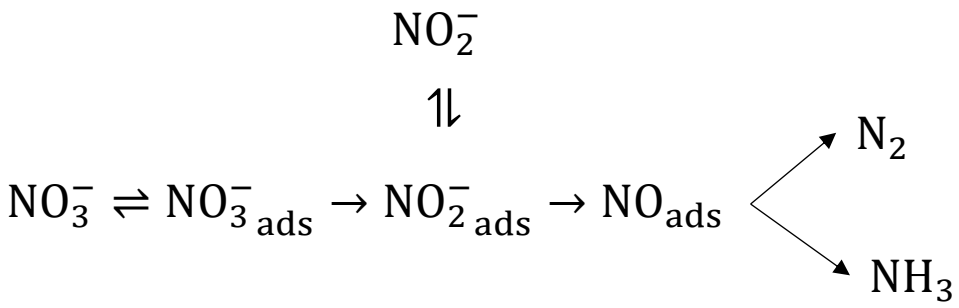


Figure 1. Reaction pathway of nitrate reduction.

It is clear that nitrate can be adsorbed on the electrodes (Duca et al., 2012). Simultaneously, $H_2O$ can be reduced on the electrode surface to form adsorbed hydrogen ($H_{ads}$). For adsorbed nitrate, it can react with $H_{ads}$ to form $NO_{2\,ads}^-$ as shown below (Lu et al., 2021):

$$H_2O + e^- \rightarrow H_{ads} + OH^-$$

$$NO_{3\,ads}^- + 2H_{ads} \rightarrow NO_{2\,ads}^- + H_2O$$

Then $NO_{2\,ads}^-$ is rapidly react with $H_{ads}$ to form $NO_{ads}$, then $N_{ads}$. Two $N_{ads}$ can combine to form $N_2$ or $N_{ads}$ can react with three $H_{ads}$ to form $NH_3$ (Duca et al.,



doi:10.6342/NTU202303029

2012; Shin et al., 2021). These reactions are shown below:

$$NO_{2\,ads}^{-} + H_{ads} \rightarrow NO_{ads}^{-} + OH^{-}$$

$$NO_{ads}^{-} + 2H_{ads} \rightarrow N_{ads} + H_2O$$

$$2N_{ads} \rightarrow N_2$$

$$N_{ads} + 3H_{ads} \rightarrow NH_3$$

Therefore, the presence of $H_{ads}$ can enhance the $NO_3^-$ conversion (Wu et al., 2022). However, Shin et al. reported that $NH_3$ was the primary product because the creation of N-H bonds by $H_{ads}$ was more active than the formation of N-N bonds. (Shin et al., 2014). To mitigate the formation of N-H for higher nitrogen gas selectivity, the use of H-affinity metal, such as Pt and Pd as the electrode material could be important (Ebbesen et al., 2010).



doi:10.6342/NTU202303029

# Chapter 3 Material and methods

## 3.1 Research framework

The research framework of this study is shown in Figure 2. Cu electrodes with different electrodeposition times and Pd/Cu bimetallic electrodes were prepared. Nitrate reduction experiments were conducted using these electrodes and the end products were analyzed to evaluate their performance.

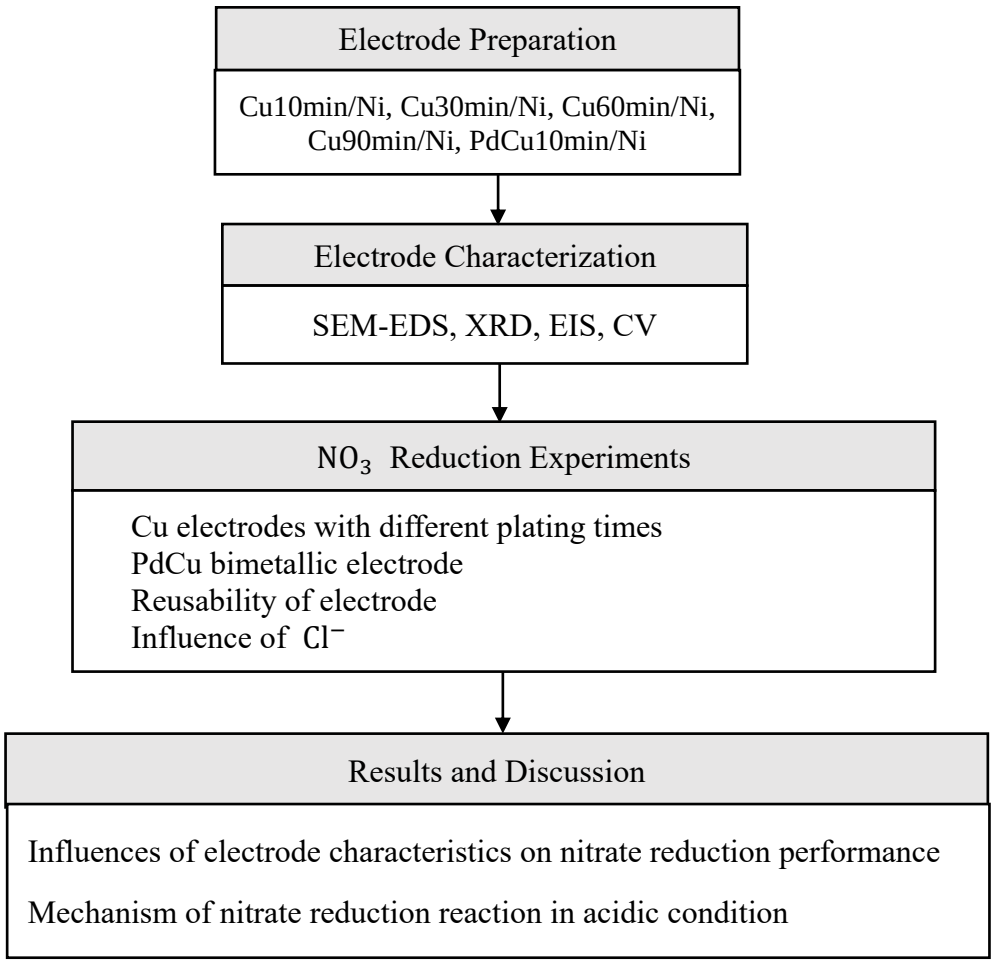


Figure 2. Research framework.



doi:10.6342/NTU202303029

### 3.2 Materials and chemicals

All electrochemical experiment was conducted using an electrochemical station under the potentiostatic and galvanostatic modes (Autolab PGSTAT204) with the NOVA 2.1 software (Metrohm, Netherlands). All electrodes were prepared by depositing the desired metals on nickel foam (Innovation Materials Co., Ltd, Taiwan) and used as the cathode in the electrochemical cell. Saturated calomel electrode (SCE) and platinum electrode were used as the reference electrode and the counter electrode, respectively.

Deionized water was obtained from PURELAB classic system (ELGA, UK). Reagent-grade chemicals were used in this study. Potassium nitrate ($KNO_3$, 99%) and sodium sulfate ($Na_2SO_4$, 99%) were purchased from Freak (Germany) and Nacalai tesque (Japan) respectively. Copper chloride ($CuCl_2$, 99%) was purchased from Alfa Aesar (USA). Palladium chloride ($PdCl_2$, 99%) was purchased from Sigma-Aldrich (USA). Hydrochloric acid (HCl, 37%), sulfuric acid ($H_2SO_4$, 95-97%), and acetone (99.5%) were purchased Honeywell-Fluka (USA). Phosphoric acid ($H_3PO_4$, 85-87%) and hypochlorite solution (NaClO, 5%) were purchased from J.T. Baker (USA).



doi:10.6342/NTU202303029

### 3.3 Electrode preparation

Nickel foam was cut into 3cm × 4cm coupons and used as the plating material for the electrodes. The nickel coupons were degreased in acetone under ultrasonic condition for 30 min, and soaked in 1M $H_2SO_4$ for 10 min to remove surface native oxides, and then washed with the deionized water for 10 min under ultrasonic condition. The cleaned nickel coupons were dried in the oven at 50℃ for 12 hr before use.

The plating bath consisted of 0.05M $CuCl_2$ and the solution pH was adjusted to 2 using $H_3PO_4$. The Ni coupon and platinum electrode were set up as the cathode and anode, respectively under the galvanostatic mode (Figure 3). Cu was electrodeposited on the Ni foam using a constant current of 30 mA/$cm^2$ with an electrodeposition time of 10, 30, 60, and 90 min and the obtained Cu electrode were named as Cu10min/Ni, Cu30min/Ni, Cu60min/Ni, and Cu90min/Ni, respectively (Figure 4(a)-4(d)).



doi:10.6342/NTU202303029

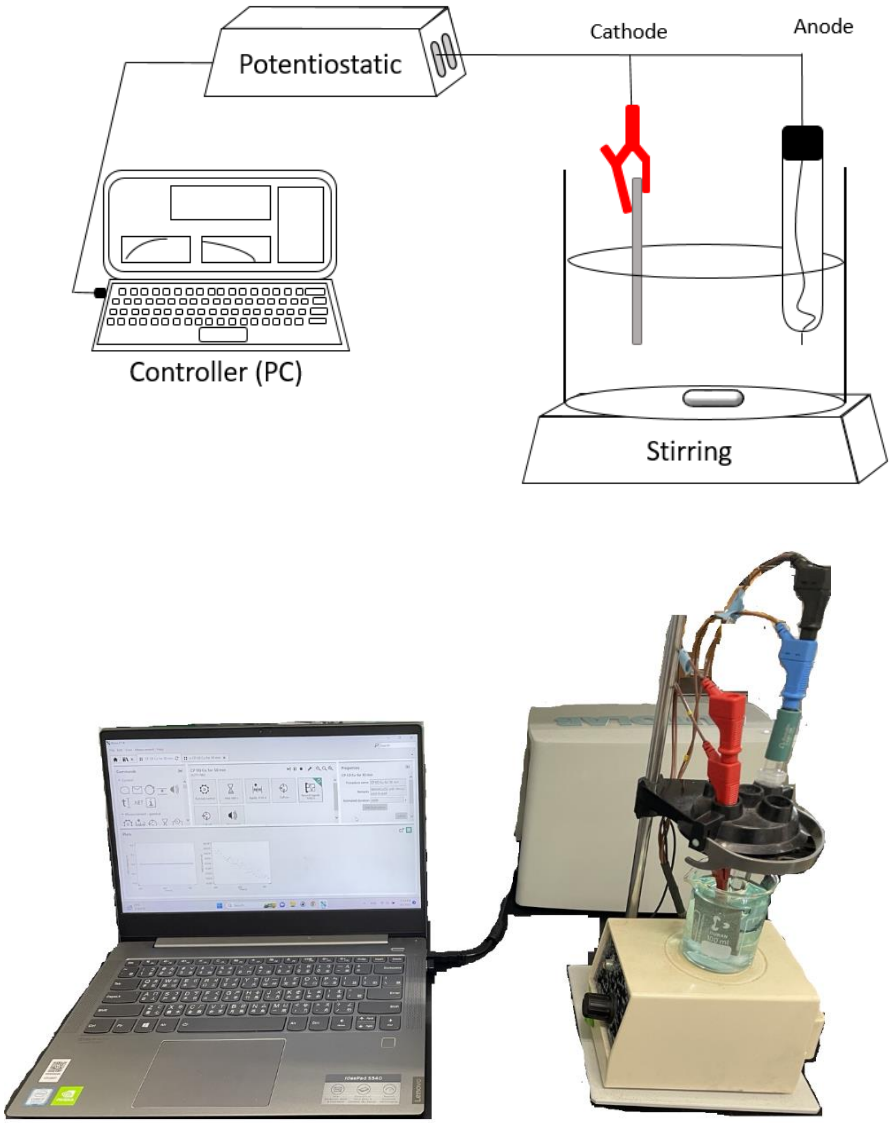


Figure 3. Schematic and picture of the galvanostat in two electrode setup.

To prepare the PdCu bimetallic electrode, the Cu10min/Ni electrode was immersed in $0.01M\ PdCl_2$ with $0.25M\ HCl$ and applied a constant current density of $20mA/cm^2$



doi:10.6342/NTU202303029

for 10 min under the two-electrode setup. Subsequently, the electrode was rinsed with acetone, washed with deionized water for several times, and then dried in oven 50℃ for 12 h.

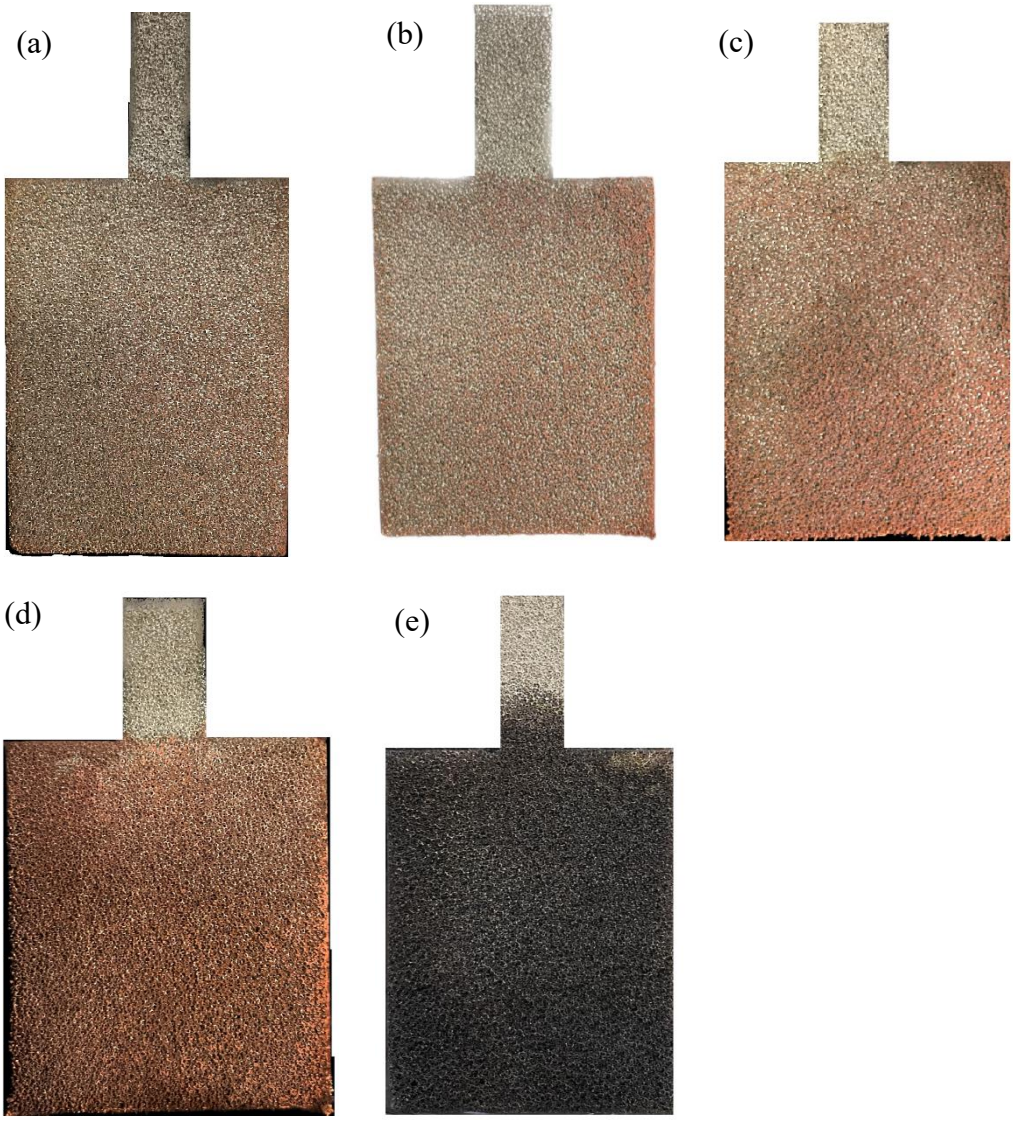


Figure 4. The picture of plated electrodes (a) Cu 10min/Ni (b) Cu30min/Ni (c) Cu60min/Ni (d) Cu90min/Ni (e) PdCu10min/Ni.



doi:10.6342/NTU202303029

### 3.4 Electrochemical nitrate reduction experiments

Electrochemical nitrate reduction experiments were carried out in an electrochemical cell under constant current mode (Figure. 3). The prepared Cu/Ni and PdCu/Ni electrodes were used as the cathode and a platinum electrode was used as the anode. Additional experiments under the constant potential mode was also carried out using the Cu10min/Ni as the cathode and the platinum electrode as the anode with the saturated calomel electrode (SCE) as the reference electrode (Fig 5). The distance between cathode and anode was 2 cm. Under the constant current mode, the solution containing 80 mg N/L $NO_3^-$ with 0.05 M $Na_2SO_4$ as the background electrolyte was used and the solution pH was adjusted to 2 by $H_3PO_4$. Under the constant potential mode, the solution containing 20 mg N/L $NO_3^-$ with $0.05M\ Na_2SO_4$ as the background electrolyte was used. To explore the influences of chloride in nitrate removal, the electrochlorination experiments under $-2V_{REF}$ constant potential were conducted.

### 3.5 Analytical methods

Scanning electron microscope energy dispersive spectrometer (SEM-EDS; JEOL JSM-7600F, Japan) was utilized to investigate the surface morphology and the elemental



doi:10.6342/NTU202303029

composition of the electrodes. X-Ray diffraction analysis (XRD; Rigaku, Japan) was used to explore the crystallographic structure and the crystallite size of deposited metals. It was operated at a scan rate of $0.33° s^{-1}$ in the incidence angle range of 20 to 80 θ. Additionally, to analyze the area facet ratio of Cu(200)/Cu(111), Origin pro 2023 software (OriginLab, USA) was used to analyze XRD data.

The concentration of $NO_3^-$, $NO_2^-$ were analyzed by ion chromatography (IC, Eco IC, Metrohm) after the sample was diluted and filtered by a 0.22 μm pore size polyvinylidene fluoride (PVDF) filter. $NH_3$ was measured by the phenate method (Standard Method 4500-$NH_3$ F). Free chlorine was measured by the DPD colorimetric method (Standard Method 4500-Cl G). The pH value was obtained by using a pH meter (SUNTEX pH meter, sp2100).

In this study, total nitrogen species shown in equation (3) was considered under acidic conditions and the generation of $N_2$ was calculated by mass balance shown in equation (4), in which at t=0, the total nitrogen was equal to $C_0(NO_3^-)$.

$$C_t(TN) = C_t(NO_3^-) + C_t(NO_2^-) + C_t(NH_4^+) \quad (3)$$

$$C_t(N_2) = C_0(NO_3^-) - [C_t(NO_3^-) + C_t(NO_2^-) + C_t(NH_4^+) + C_t(\text{Combined Chlorine})] \quad (4)$$



doi:10.6342/NTU202303029

To evaluate nitrate reduction rate, k, it was calculated by assuming the pseudo-first order.

$$-\frac{dC_{NO_3^-}}{dt} = kC_{NO_3^-} \quad (5)$$

Where $C_{NO_3^-}$ is the $NO_3^-$ concentration (unit of mg N/L), t is reaction time (unit of min).



doi:10.6342/NTU202303029

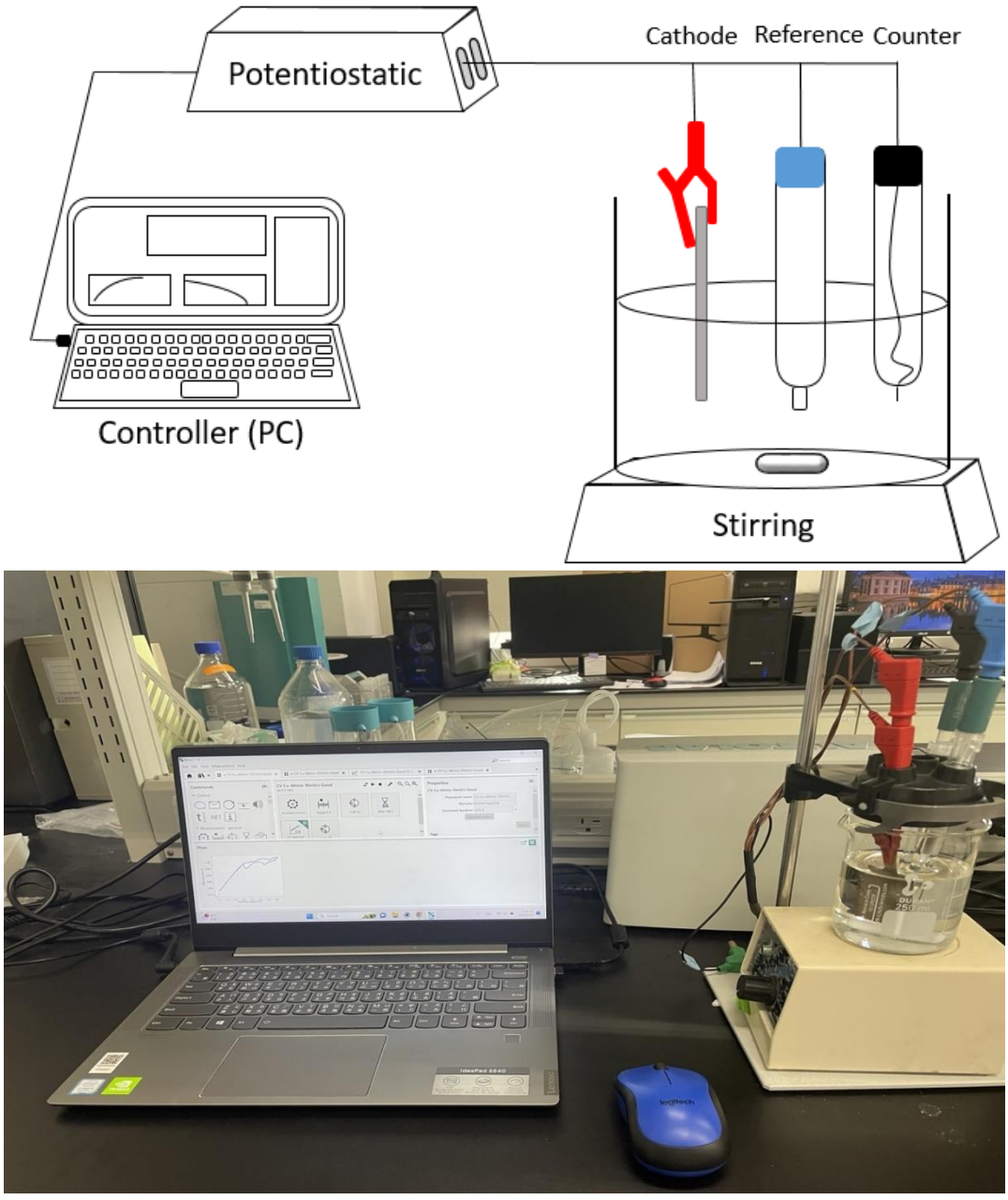


Figure 5. Schematic and picture of the potentiostatic in three electrode setup.



doi:10.6342/NTU202303029

# Chapter 4 Results and Discussion

## 4.1 Characterization of electrodes

Figure 6 shows the SEM images of copper electrodes prepared by different plating times from 10 min to 90 min. Ni foam was shown as the skeletons with interconnecting pores. The plated copper particles tended to agglomerate and exhibited a granule shape. The size of Cu granules increased and led to the generation of a rhombus structure with the increasing plating time.

The SEM image and elemental distribution for PdCu10min/Ni are shown in Figure 7. After the two-step plating process, the surface of the PdCu10min/Ni electrode exhibited a grape-cluster-like shape with pores. The palladium particles were found to accumulate on the surface of copper.

To investigate the elemental compositions of the prepared electrodes, the atomic ratio of different elements obtained by the EDS are shown in Figure 8. It was found that the proportion of Cu increased with the increasing plating time. Furthermore, Ni was not detected for Cu60min/Ni and Cu90min/Ni, indicating that Cu particles had completely covered the nickel foam surfaces for these two electrodes.



doi:10.6342/NTU202303029

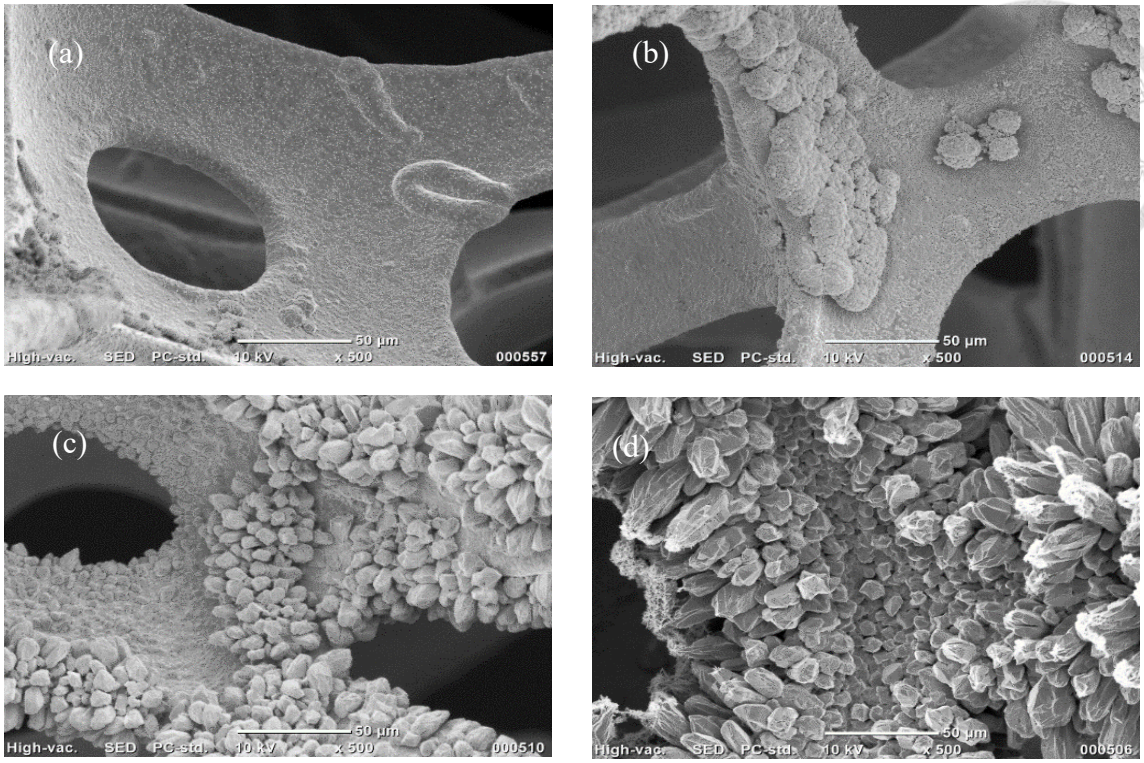


Figure 6. SEM images of (a) Cu10min/Ni (b) Cu30min/Ni (c) Cu60min/Ni (d) Cu90min/Ni.

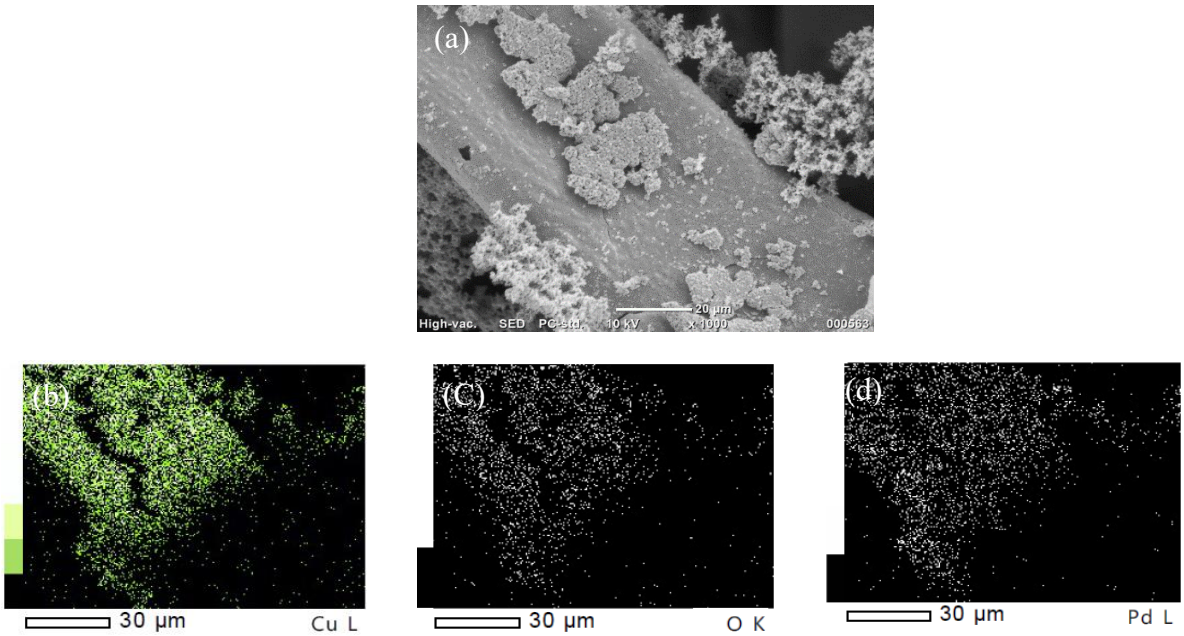


Figure 7. (a) SEM image of PdCu10min/Ni (x1000), and the elemental distributions of (b) copper, (c) oxygen and (d) palladium, respectively.



doi:10.6342/NTU202303029

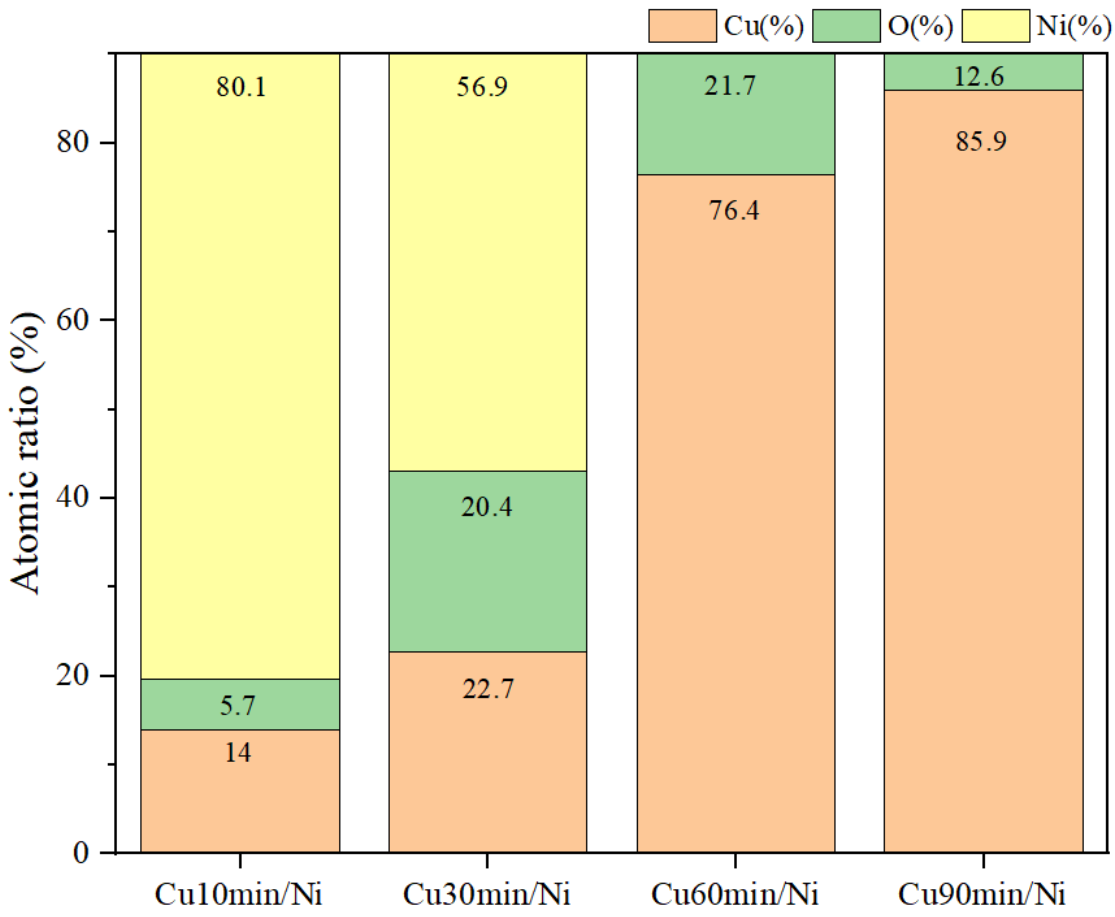


Figure 8. The atomic ratios of different elements in the electrodes determined using the EDS.

The XRD patterns of the prepared electrodes are shown in Figure 9. The diffraction peaks of Cu, Pd and Ni metals could be clearly seen. Specifically for Cu, the facets of Cu(111) and Cu(200) could be distinguished by the two peaks at $2\theta = 43.5°$ and $50.7°$, respectively. It is clear that the intensities of Cu(111) and Cu(200) increased with the



doi:10.6342/NTU202303029

increasing plating time. The intensity of Pd at $2\theta = 40.1°$ indicated the facet of Pd(111) formed on the PdCu10min/Ni electrode.

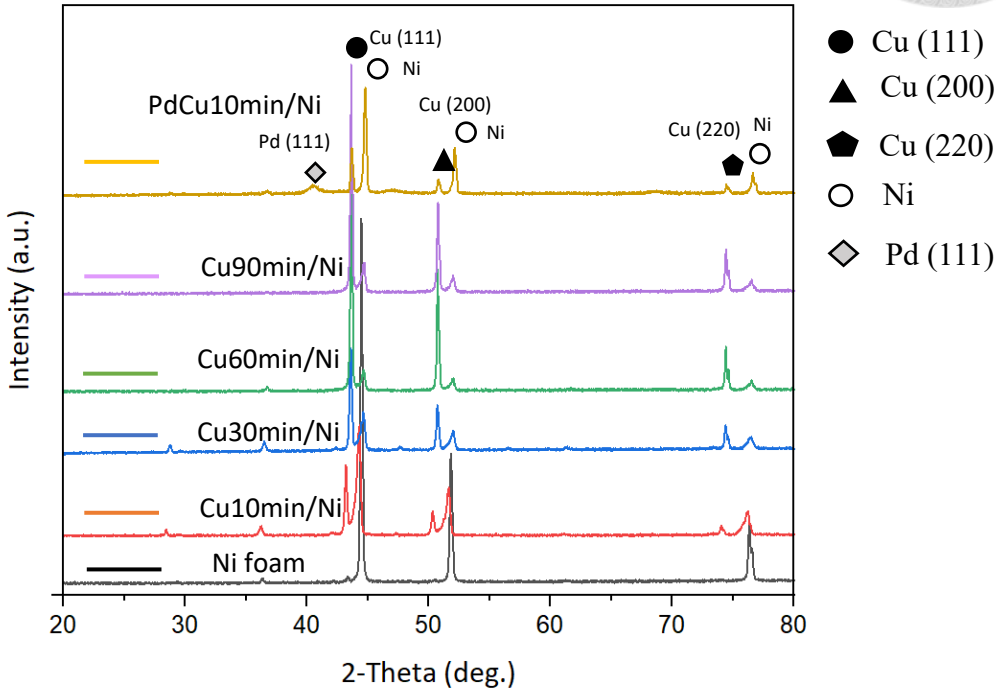


Figure 9. XRD patterns of the prepared electrodes.

Figure 10 (a) shows the ratio of Cu(200)/Cu(111) by different plating times. The ratio gradually increased with the increasing plating time and reached 0.5 at 90 min plating time. It has been reported that copper ion was dominantly deposited on the top of the vertically covered supporting matrix due to a shorter diffusion distance (Lee et al., 2016). This could lead to a greater tendency for copper ion to adsorb on the top of Cu (111) followed by reduction to Cu (200) leading to a higher Cu (200)/Cu (111) ratio when the



doi:10.6342/NTU202303029

plating time increases.

Figure 10 (b) shows the crystallite size of the particles plated on the electrodes determined according to the Scherer equation (Equation (6)).

$$D = \frac{k\lambda}{\beta cos\theta} \tag{6}$$

where, D = crystallites size (nm), k = 0.9 (Scherer constant), $\lambda$ = 0.15406 nm (Wavelength of the x-ray sources), $\beta$ = Full Width at Half Maximum, FWHM (radians), and $\theta$ = Peak position (radians).



doi:10.6342/NTU202303029

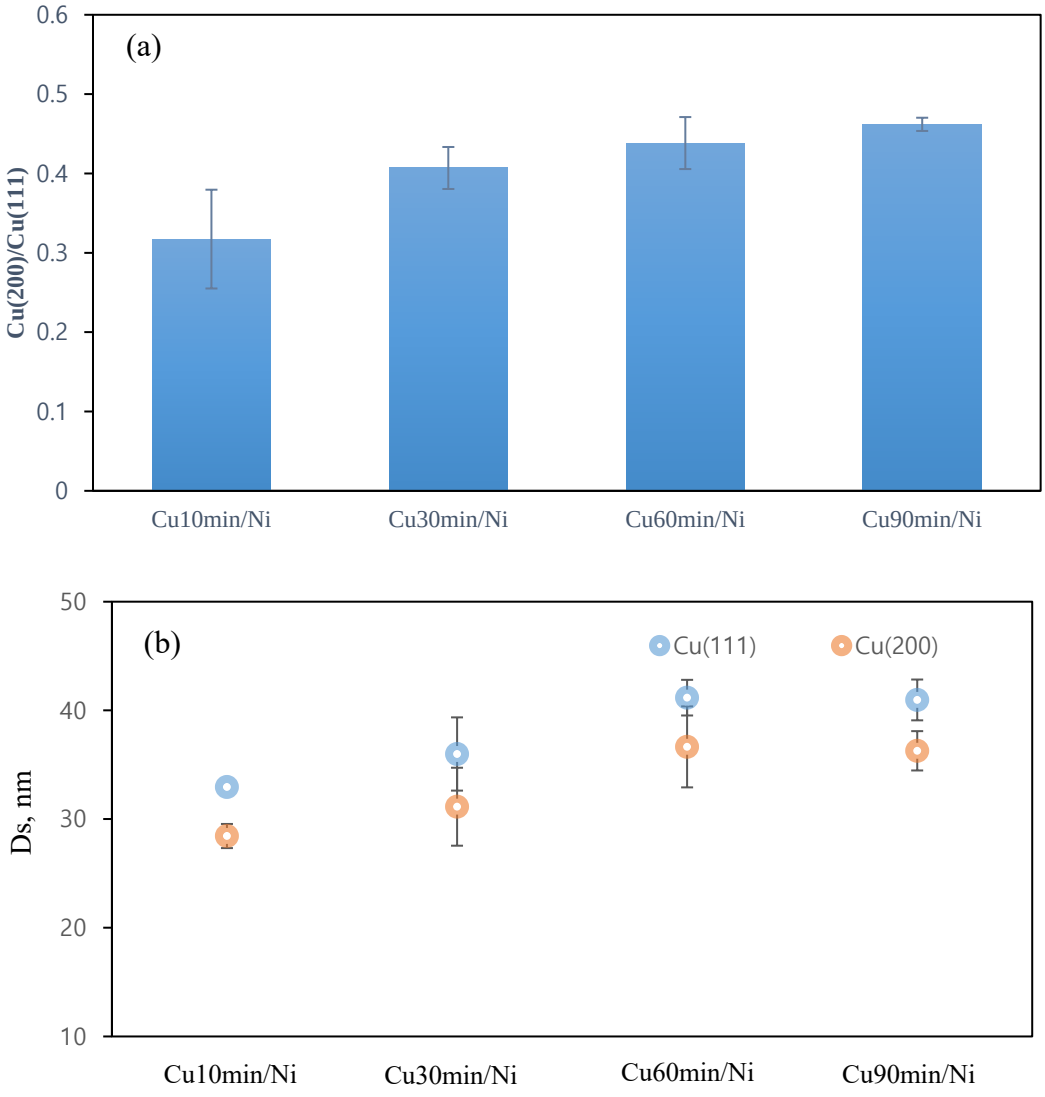


Figure 10. XRD analysis of (a) area ratio of Cu(200)/Cu(111) (b) crystal size.

The crystallite sizes of Cu(111) and Cu(200) increased with the increasing plating time and reached the maximum sizes of 41.2 nm and 36.6 nm, respectively when the plating time was 60 min. Increasing plating time can initiate the aggregation of granules,



doi:10.6342/NTU202303029

which increases the particle size of the Cu crystals.

Electrochemical Impedance Spectroscopy (EIS) was used to investigate the electrochemical properties of the electrodes. The obtained Nyquist plots are presented in Figure 11. In this study, the equivalent circuit based on the Randles-like model was considered (Sun et al., 2002). The determined charge transfer resistances, $R_{ct}(\Omega)$, are summarized in Table 1. The $R_{ct}(\Omega)$ decreased with the increasing plating time for monometallic Cu electrodes, with the minimum of 76.7 Ω for the Cu90min/Ni electrode. For PdCu 10min/Ni bimetallic electrode, an even smaller $R_{ct}(\Omega)$ was found (26.4 Ω), indicating that the presence of Pd significantly improved the electron transfer ability for the electrode.



doi:10.6342/NTU202303029

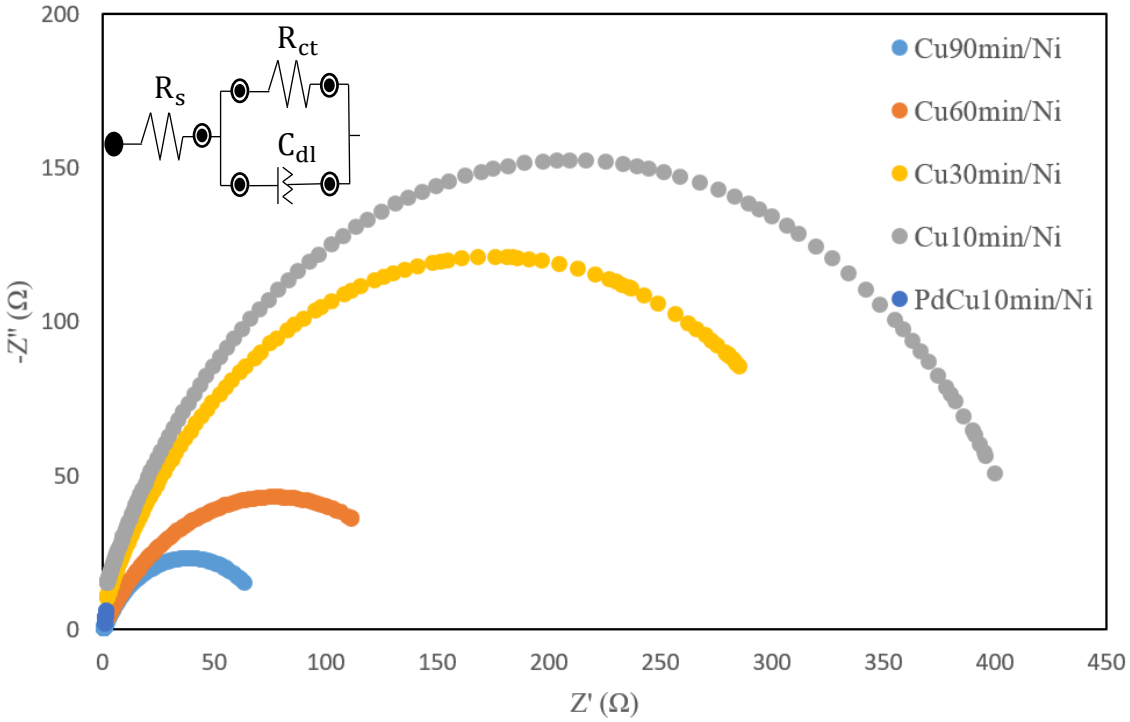


Figure 11. The Nyquist curve for different electrodes. The Randles-like model was considered. $\mathbf{Rs}$, $\mathbf{R_{ct}}$, $\mathbf{C_{dl}}$ represents the solution resistance, the charge transfer resistance, and the double layer capacitance, respectively.

Table 1. The results of $\mathbf{R_{ct}}$ (Ω) for different electrodes

| | $R_{ct}$ (Ω) |
|---|---|
| Cu10min/Ni | 429.0 |
| Cu30min/Ni | 354.8 |
| Cu60min/Ni | 154.7 |
| Cu90min/Ni | 76.7 |
| PdCu10min/Ni | 26.4 |



doi:10.6342/NTU202303029

The electrochemical active surface area (ECSA) can be utilized to compare electrocatalyst activity by different plating times. The double-layer capacitance, $C_{dl}$, and the specific capacitance of the electrode material, $C_s$, can be used to determine ECSA. according to equation (7)

$$ECSA=\frac{C_{dl}}{C_s} \quad (7)$$

However, determining the precise capacitance for precise evaluation of ECSA presents a challenge, since its calculation depends on factors such as electrode potential, surface structure, and the composition/concentration of the electrolyte. Thereby, a widespread consensus for the specific capacitance value is difficult to achieve even using the same material (Wei et al., 2019). Since the specific capacitance is frequently unknown, it has been common to utilize a single $C_s$ value to determine ECSA for different materials, in spite of the composition of the electrodes, which inevitably results in significantly underestimation or overestimation of ECSA values (Connor et al., 2020). It has recently been suggested that, the net measured current, and the current normalized by geometric area and double layer capacitance $C_{dl}$ could be used to display the catalytic activity instead of ECSA. (Masa et al., 2020). Hence, although $C_s$ is unknown, monitoring $C_{dl}$ allowed for the determination of relative changes in ECSA.



doi:10.6342/NTU202303029

The double layer capacitance for different electrodes was determined using the cyclic voltammetry (CV) at various scan rates from $10\ \mathrm{mV/s}$ to $120\ \mathrm{mV/s}$ in non-faradic region from $-0.3\mathrm{V}$ to $-0.5\mathrm{V}$, as shown in Figure 12. Firstly, the peak current density ($\Delta \mathrm{j}$, equation (11)) was obtained from the CV chart (Figure 12). Subsequently, the obtained $\Delta \mathrm{j}$ was plotted versus the scan rate of CV chart according to Equation (9).

$$\Delta \mathrm{j} = \mathrm{j}_{\mathrm{p,anodic}} - \mathrm{j}_{\mathrm{p,cathodic}} \tag{8}$$

$$\mathrm{C}_{\mathrm{dl}} = \frac{\Delta \mathrm{j}}{\mathrm{V}} \tag{9}$$

where, $\mathrm{J}$ is the current density, $\mathrm{mA/cm^2}$, $\mathrm{v}$ is the scan rate, mV/s.

Figure 13 shows the slopes of these plots which indicates the double-layer capacitance ($\mathrm{C_{dl}}$) of the electrodes. The obtained $\mathrm{C_{dl}}$ is shown in Table 2. The smallest $\mathrm{C_{dl}}$ value ($2.58\ \mathrm{mF/cm^2}$) was found for Cu10min/Ni. The double layer capacitance gradually increased with the plating time and reached $5.53\ \mathrm{mF/cm^2}$ for Cu90min/Ni. It is clear that by extending plating time for Cu, the double layer capacitance would increase.



doi:10.6342/NTU202303029

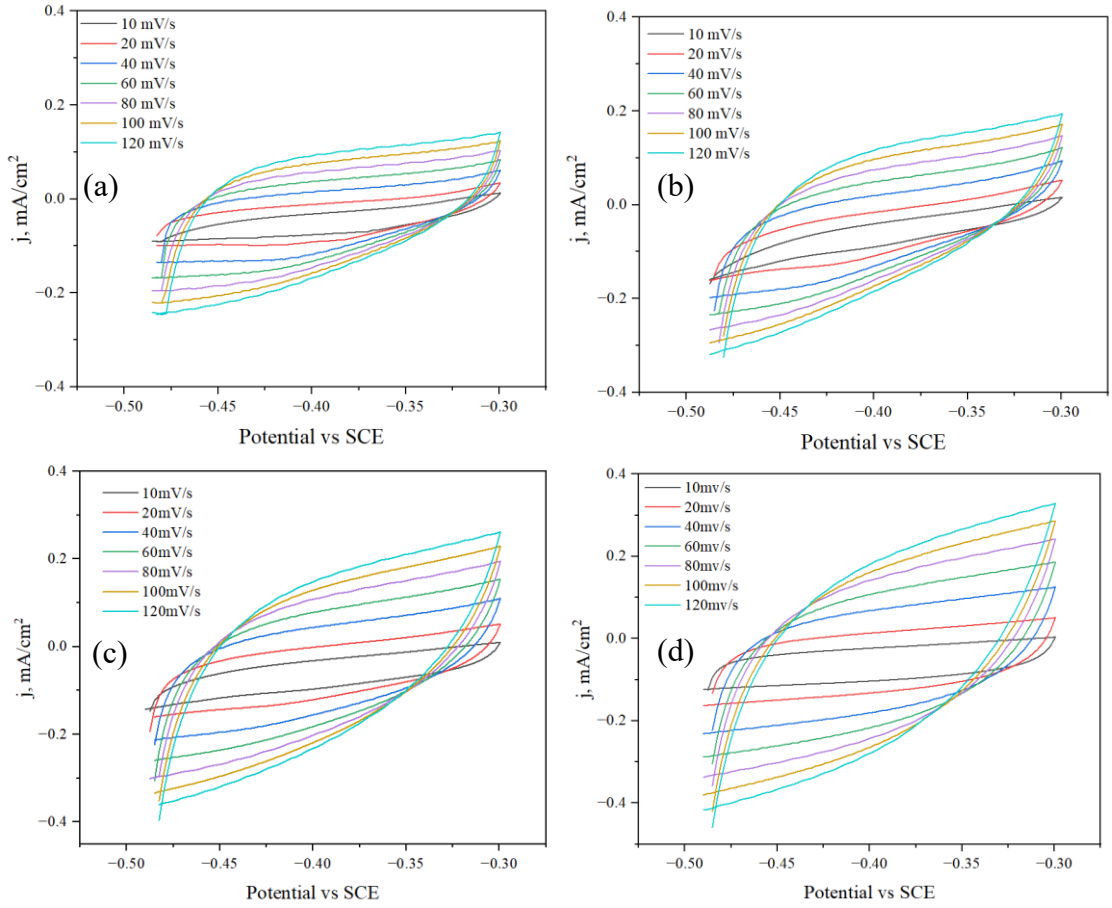


Figure 12. Cyclic voltammetry of (a) Cu10min/Ni, (b) Cu30min/Ni, (c) Cu60min/Ni, (d) Cu90min/Ni in the range of $\mathbf{-0.5\,V}$ to $\mathbf{-0.2\,V}$ in the presence of 0.05M $\mathbf{Na_2SO_4}$. The scan rate was changed from $\mathbf{10m\,V/s}$ to $\mathbf{120\,mV/s}$.



doi:10.6342/NTU202303029

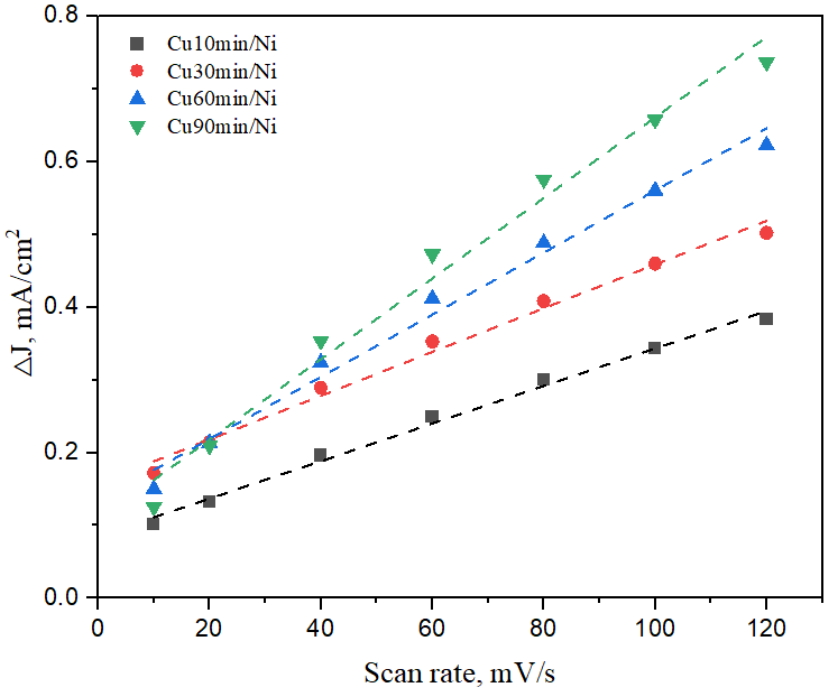


Figure 13. Charging current density versus scan rate.

Table 2. The fitting results of current density versus scan rate.

| | Cu10min/Ni | Cu30min/Ni | Cu60min/Ni | Cu90min/Ni |
|---|---|---|---|---|
| $C_{dl}$ (mF/cm$^2$) | 2.6 | 3.0 | 4.3 | 5.5 |



doi:10.6342/NTU202303029

## 4.2 Nitrate reduction performance of different electrodes

### 4.2.1 Nitrate reduction performance under a constant current density

Figure 14 shows the nitrate reduction as a function of time using Cu monometallic electrodes under a constant current density 20 $mA/cm^2$. The experimental solution had an initial $[NO_3^-] = 80$ ppm as N and initial pH=2 with $0.05M\ Na_2SO_4$ as the inert electrolyte. All Cu monometallic electrodes showed excellent nitrate removal ability, in which after 240 min almost all $NO_3^-$ were removed. The pseudo-first order rate constant for Cu10min/Ni, Cu30min/Ni, Cu60min/Ni, and Cu90min/Ni were 0.00981, 0.01285, 0.01523, and $0.02min^{-1}$, respectively and the coefficient $R^2$ were all higher than 0.98 (Figure 16 and Table 3). This observation was consistent the charge transfer resistance $R_{ct}\ (\Omega)$ results presented in Table 1 and the double-layer capacitance $(C_{dl})$ results presented in Table 2, i.e., the electrode with a longer Cu plating time would have a lower $R_{ct}\ (\Omega)$ and a higher $C_{dl}$ to facilitate the rate of electron transfer for the reduction of nitrate. The main product for nitrate reduction was $NH_4^+$. $NO_2^-$ was not detected in all experiments. It is likely that $NO_2^-$, if formed as an intermediate, is very reactive on the Cu metal surface and rapidly convert to $NH_4^+$ (Dima et al., 2003; Iwamoto, 2017). Even though all Cu monometallic electrodes exhibited good performance for nitrate reduction,



doi:10.6342/NTU202303029

no $N_2$ was generated under the acidic conditions.

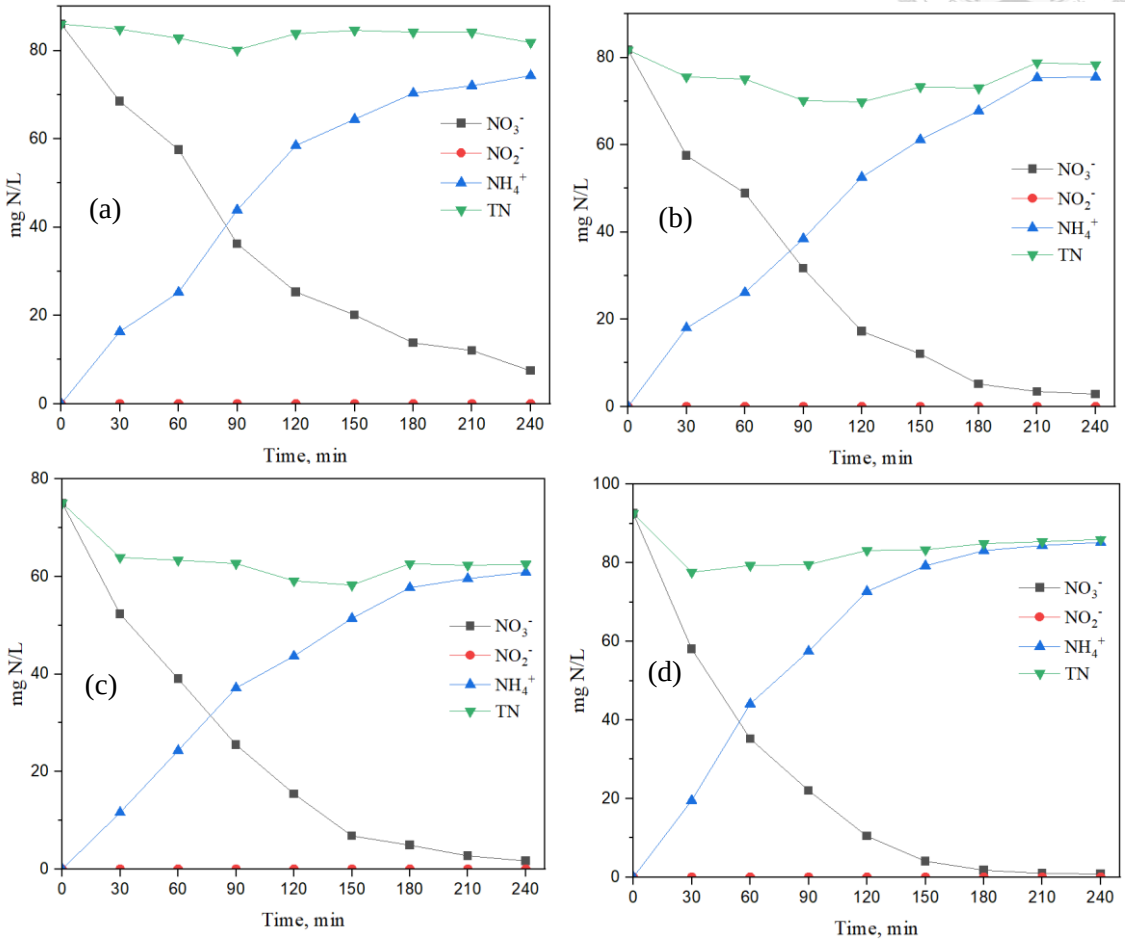


Figure 14. The concentration of $\mathbf{NO_3^-}$, $\mathbf{NO_2^-}$, and $\mathbf{NH_4^+}$ as a function of time in nitrate reduction experiments using (a) Cu10min, (b) Cu30min, (c) Cu60min, and (d) Cu90min (constant current density $\mathbf{20mA/cm^2}$, $\mathbf{0.05M\ Na_2SO_4}$, initial $\mathbf{NO_3^-}$ $\mathbf{80\ mg\ N/L}$, pH = 2).



doi:10.6342/NTU202303029

Figure 15 shows the nitrate reduction as a function of time using PdCu10min/Ni bimetallic electrode under a constant current 20 $mA/cm^2$. The pseudo-first order rate constant for nitrate reduction was $0.02434 min^{-1}$, which was higher than the rate constants of all Cu monometallic electrodes (Figure 16 and Table 3). This result is consistent with its lower $R_{ct}$ $(\Omega)$ and higher $C_{dl}$ when compared to those of Cu monometallic electrodes (Table 1 and Table 2). This could be attributed to the fact that palladium metal has a high ability to absorb hydrogen ions which can accelerate the indirect nitrate reduction (Duncan et al., 2008, Sun et al., 2012). Again, $NH_4^+$ was the dominant product and no $N_2$ was generated under the acidic condition when the PdCu bimetallic electrode was used.



doi:10.6342/NTU202303029

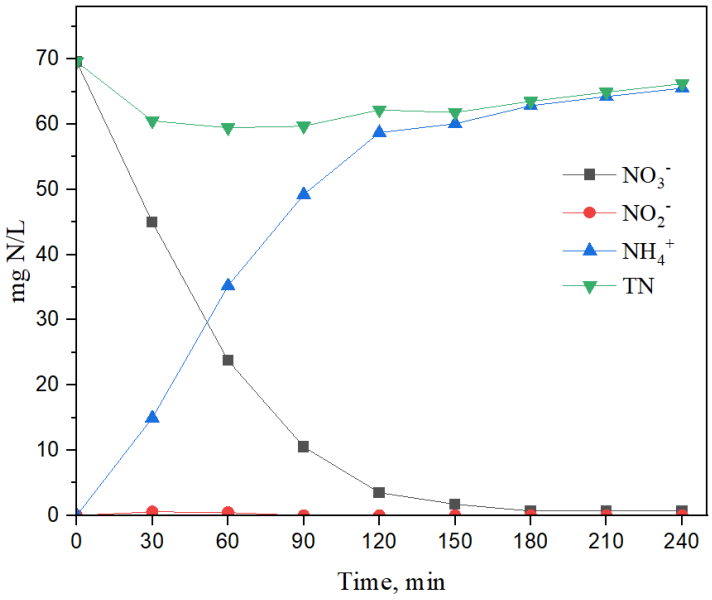


Figure 15. The concentration of $\mathbf{NO_3^-}$, $\mathbf{NO_2^-}$, and $\mathbf{NH_4^+}$ as a function of time in nitrate reduction experiments using CuPd 10min/Ni (constant current density $\mathbf{20\ mA/cm^2}$, $\mathbf{0.05M\ Na_2SO_4}$, initial $\mathbf{NO_3^-} \sim \mathbf{70\ mg\ N/L}$, pH = 2).



doi:10.6342/NTU202303029

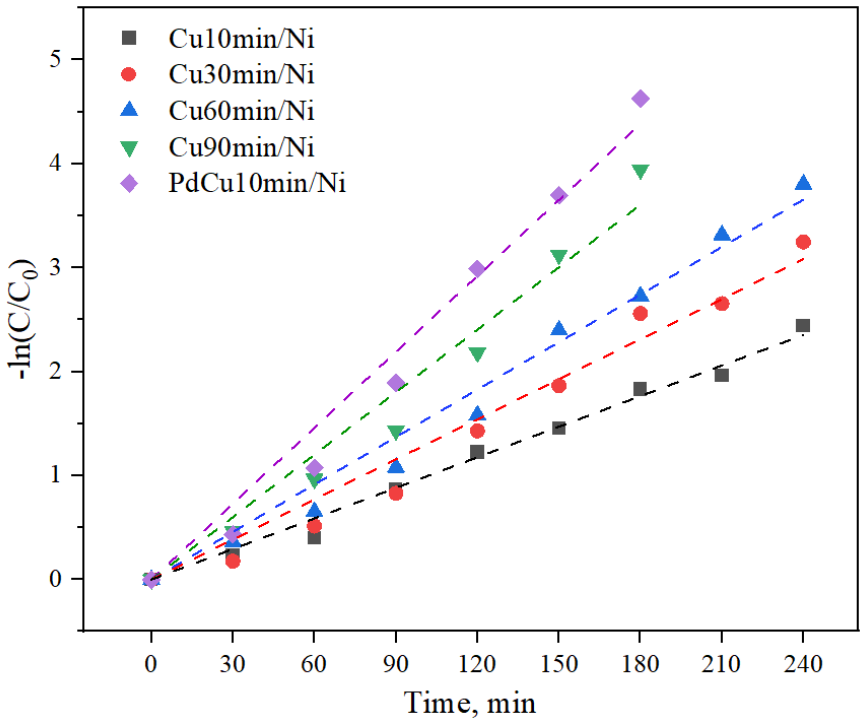


Figure 16. Fitting results of the pseudo-first-order kinetic model.

Table 3. Fitting results of the pseudo-first-order kinetic model for different cathodes.

| | Cu10min/Ni | Cu30min/Ni | Cu60min/Ni | Cu90min/Ni | PdCu10min/Ni |
|---|---|---|---|---|---|
| $k$, $\mathrm{min}^{-1}$ | 0.00981 | 0.01285 | 0.01523 | 0.02 | 0.02434 |
| R-square | 0.996 | 0.988 | 0.993 | 0.986 | 0.991 |



doi:10.6342/NTU202303029

4.2.2 Nitrate reduction performance under constant potential

Nitrate reduction performance under constant potential was evaluated to further investigate the selectivity of $NH_4^+$ and $N_2$ for the prepared electrodes. Before the experiments, the cyclic voltammetry (CV) curves under a scan rate of 10 mV/s were constructed using Cu10min/Ni electrode to investigate the overpotential in terms of nitrate reduction following the IUPAC as shown in Figure 17 (Elgrishi et al., 2017). Solutions with $NO_3^-$ (20 mgN/L $NO_3^-$) and without $NO_3^-$ were used. In the absence of $NO_3^-$, the oxidative corrosion for $Cu^0$ had one peak potential ($O_1$) at $-0.29V$ vs SCE which can be attributed to the formation of copper oxide as shown in the following reaction.

$O_1$: $Cu^0 + H_2O \rightarrow CuO(s) + 2H^+ + 2e^-$

In terms of the reduction, two peaks at $-0.55V$ ($R_1$) and $-0.17V$ ($R_2$) were found, suggesting that the reduction of copper oxide proceeded with two one-electron steps as shown below.

$R_1$: $Cu^+ + e^- \rightarrow Cu^0$

$R_2$: $Cu^{2+} + 2e^- \rightarrow Cu^0$



doi:10.6342/NTU202303029

In the presence of nitrate, the additional $R_N$ current appeared, suggesting that nitrate reduction reaction involving the oxidation of $Cu^0$ at $-0.6V$ vs SCE.

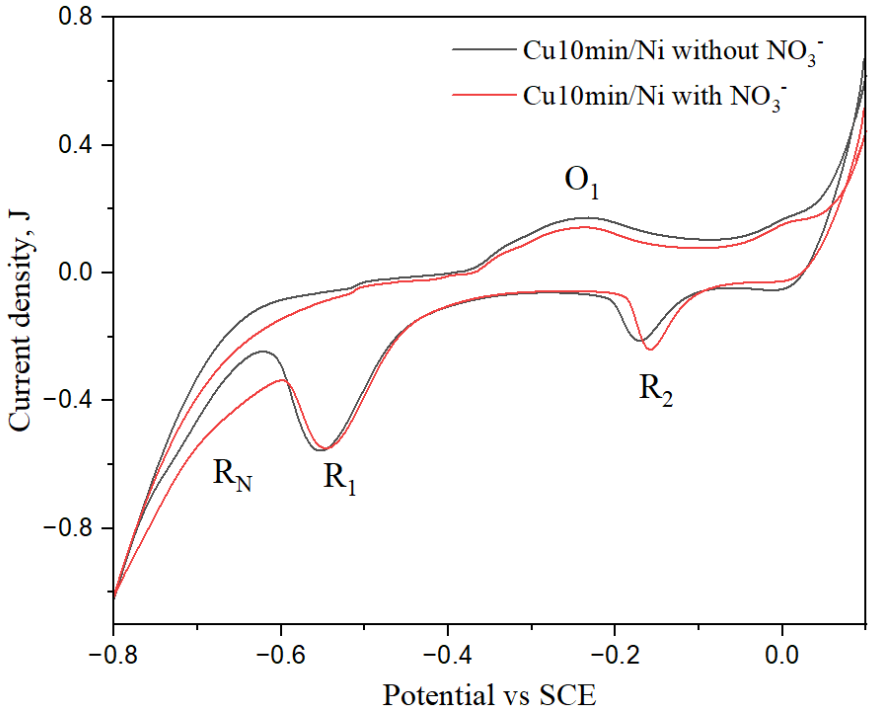


Figure 17. Cyclic voltammetry curve of Cu10min/Ni scanned in the range of $\mathbf{-0.8V}$ to $\mathbf{0.1V}$ in the absence and presence of $\mathbf{20\ mg\ N/L\ NO_3^-}$.

According to the CV curves, the overpotential was selected in the range of $-0.6V$ to $-0.9V$ vs SCE for nitrate reduction and the results are shown in Figure 18. The experimental solution had an initial $[NO_3^-] = 20$ ppm as N and initial $pH = 2$ with $0.05M\ Na_2SO_4$ as the inert electrolyte. By applying a low potential of $-0.6V$, only



doi:10.6342/NTU202303029

small amount of nitrate was converted to ammonia ion, $NH_4^+$. By increasing the overpotential to $-0.9V_{REF}$, $NO_3^-$ was completely converted to $NH_4^+$ under the acidic condition. No $N_2$ was generated in these overpotentials. The pseudo-first order rate constants determined for $-0.6V_{REF}$, $-0.7V_{REF}$, $-0.8V_{REF}$, and $-0.9V_{REF}$ were 0.00104, 0.00375, 0.00791, 0.0213$min^{-1}$, respectively (Table 4).



doi:10.6342/NTU202303029

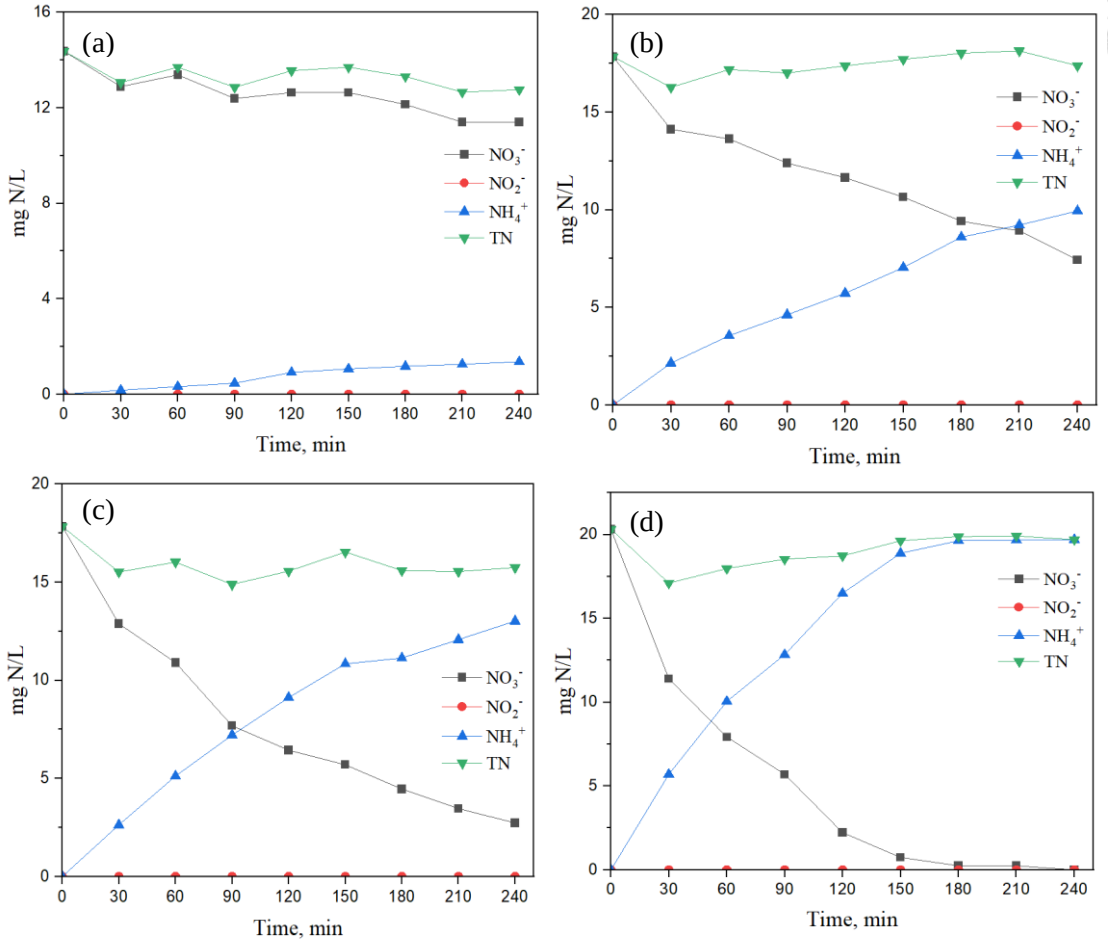


Figure 18. Nitrate reduction reaction on Cu10min/Ni under the different constant potential (constant potential (a)$-\mathbf{0.6V_{REF}}$, (b)$-\mathbf{0.7V_{REF}}$, (c)$-\mathbf{0.8V_{REF}}$, (d)$-\mathbf{0.9V_{REF}}$, $\mathbf{0.05M\ Na_2SO_4}$, initial $\mathbf{NO_3^-}$ ~ **20 mg N/L**, pH = 2).

.



doi:10.6342/NTU202303029

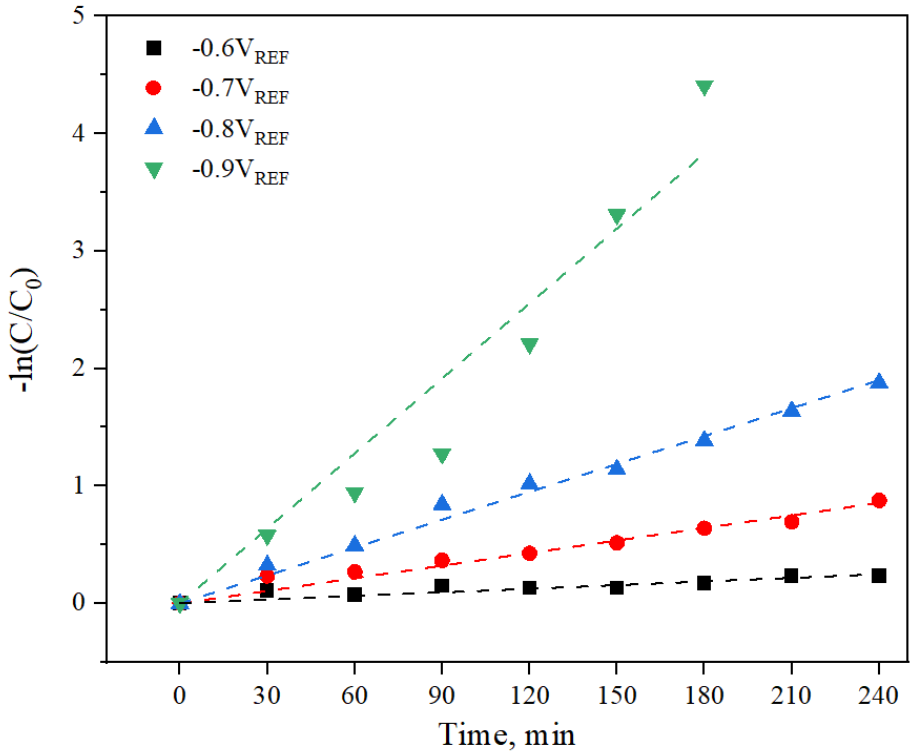


Figure 19. Fitting results of the pseudo-first-order kinetic model

Table 4. Fitting results of the pseudo-first-order kinetic model for different potentials.

| | $-0.6V_{REF}$ | $-0.7V_{REF}$ | $-0.8V_{REF}$ | $-0.9V_{REF}$ |
|---|---|---|---|---|
| $k$, $min^{-1}$ | 0.00104 | 0.00375 | 0.00791 | 0.0213 |
| R-square | 0.942 | 0.988 | 0.99 | 0.97 |



doi:10.6342/NTU202303029

### 4.3 Reusability of Cu electrode

To investigate the reusability of Cu electrodes, Cu90min/Ni was chosen due to its superior nitrate removal efficiency compared to other electrodes. After each experiment, the electrode was thoroughly rinsed with DI water and dried at 60℃ in an oven for 10 hr before the next test. Figure 20 shows the nitrate reduction performance of the electrode for four successive experiments. Consistent removal of $NO_3^-$ and formation of $NH_4^+$ was found in all experiments although the electrode surface started to experience scratching starting from the third experiment due to the high stirring rate of 400 rpm used in the experiment.



doi:10.6342/NTU202303029

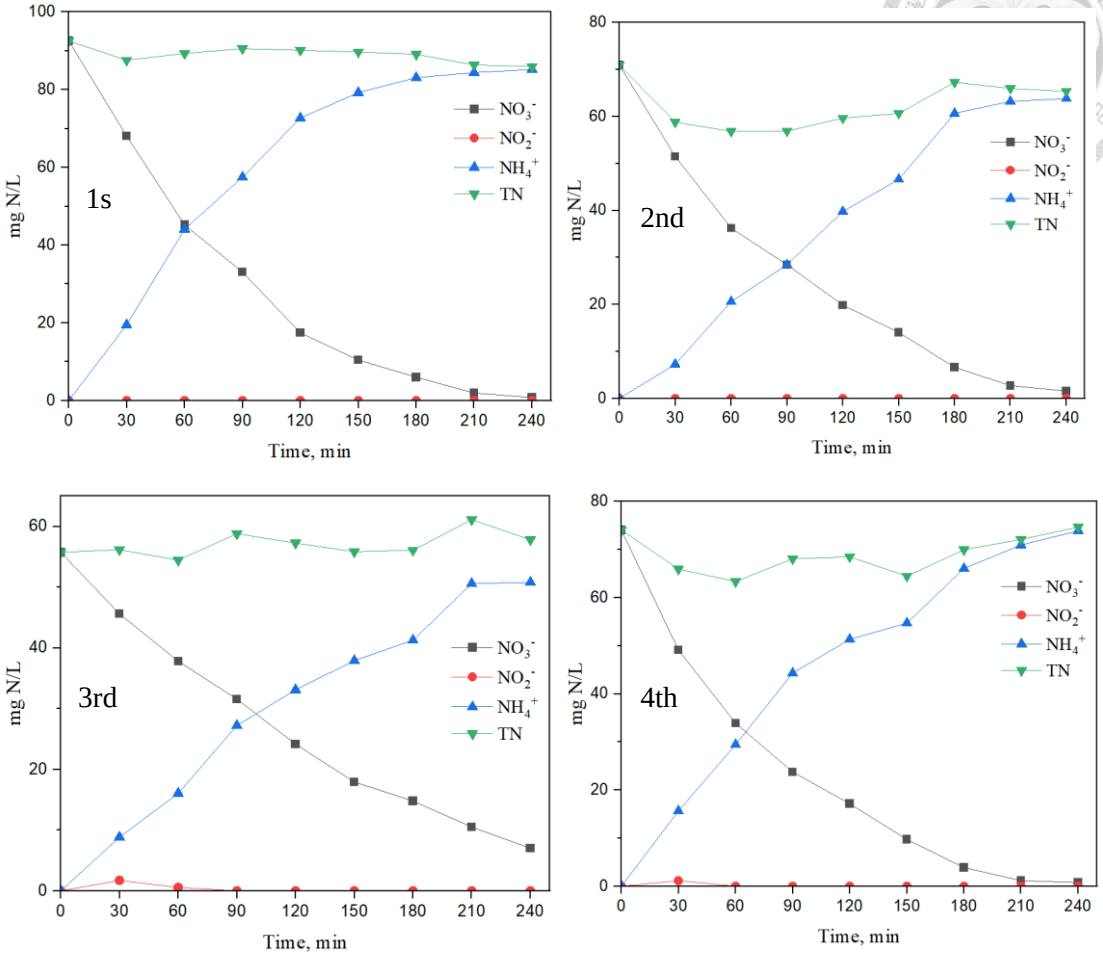


Figure 20. The concentration of $\mathbf{NO_3^-}$, $\mathbf{NO_2^-}$, and $\mathbf{NH_4^+}$ as a function of time in four successive nitrate reduction experiments using Cu90min/Ni electrode (constant current density $\mathbf{20mA/cm^2}$, $\mathbf{0.05M\ Na_2SO_4}$, initial $\mathbf{NO_3^-}$ **~ 75 mg N/L**, pH=2).



doi:10.6342/NTU202303029

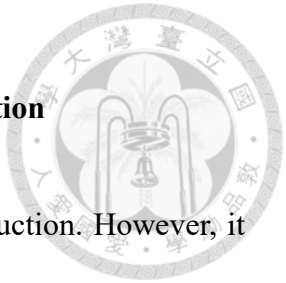

### 4.4 Enhancement of Nitrogen gas evolution using electrochlorination

Formation of $N_2$ is preferred in the electrochemical nitrate reduction. However, it was found that the formation of ammonia is more favorable in this study as well as in others (Teng et al., 2022, Lu et al., 2021). To mitigate the generation of $NH_3$ in the nitrate reduction, electrochlorination process has been proposed (Garcia-Segura et al., 2018).

The electrochlorination process involves the oxidation of chloride ion ($Cl^-$) to form hypochlorous acid ($HOCl^-$) on the anode and excess hypochlorous acid can oxidize $NH_3$ resulting from nitrate reduction to form $N_2$ based on breakpoint chlorination as shown in the following reactions (Mostafa et al., 2018).

$$Cl_{2(g)} + 2e^- \leftrightharpoons 2Cl^-,\ E^0 = 1.36V \text{ vs NHE} \quad (10)$$

$$Cl_2 + H_2O \leftrightharpoons HOCl + HCl \quad (11)$$

$$2NH_3 + 3HClO \rightarrow N_2 + 3H_2O + 3H^+ + 3Cl^- \quad (12)$$

Therefore, various $Cl^-$ concentrations (including $0.05M$, $0.1M$, $0.2M$ NaCl was added to investigate the enhancement of $N_2$ evolution using electrochlorination. The following experimental condition was employed: $NO_3^- = 40$ ppm as N, $pH = 5$, $Na_2SO_4 = 0.05$ M as an inert electrolyte, and a constant potential, $-2V_{REF}$. The reason why pH 5 was selected was to ensure the formed chlorine gas would effectively dissolve



doi:10.6342/NTU202303029

in the solution (Gombas et al., 2017). The obtained results are shown in Figure 21. It was found that the generation of $NH_4^+$ was alleviated to some extent in the presence of 0.05M NaCl. By increasing the $Cl^-$ concentration to 0.1M, high amount of hypochlorous acid generated on the anode could totally convert $NH_4^+$ to $N_2$ in 120 min. When $Cl^-$ concentration further increased to 0.2 M, the conversion could be completed in 60 min. In terms of chlorine species, including combined chlorine and free chlorine, these were detected only the small amounts of free chlorine and combined chlorine (< 2 mg/L) were detected in the presence of 0.1M and 0.2M NaCl. It should be noted that hypochlorous acid could receive electron from the cathode and reduced to $Cl^-$ (Ordeig et al., 2005).



doi:10.6342/NTU202303029

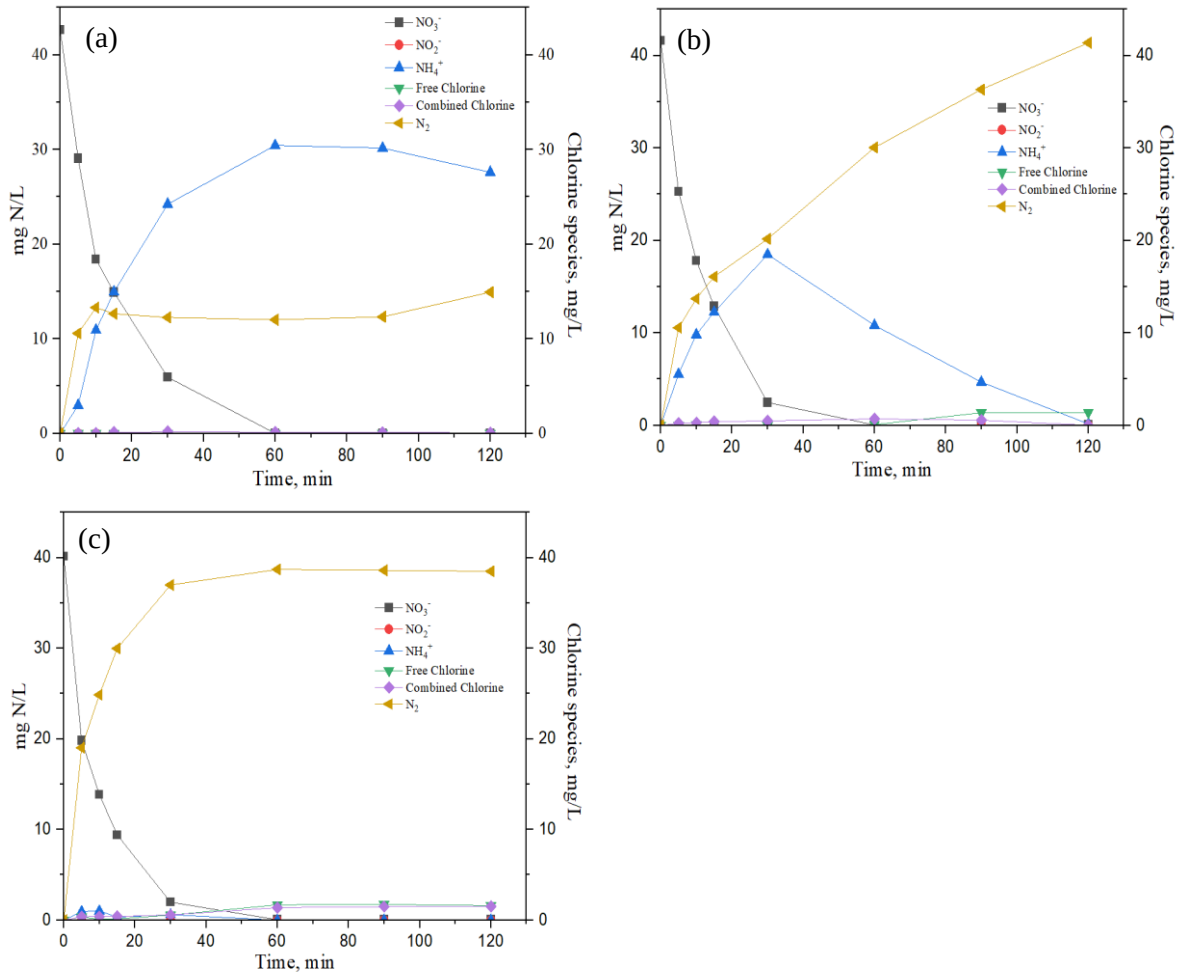


Figure 21. Enhancement of nitrogen gas evolution using electrochlorination in the presence of different NaCl concentration (a) $\mathbf{0.05M}$, (b) $\mathbf{0.1M}$, (c) $\mathbf{0.2M}$ (Constant potential: $\mathbf{-2V_{REF}}$, $\mathbf{40\ mg\ N/L\ NO_3^-}$, $\mathbf{0.05M\ Na_2SO_4}$, pH=5).



doi:10.6342/NTU202303029

# Chapter 5 Conclusions and Recommendations

In this research, the plating of Cu and Pd on Ni foam was performed using varying plating times and the electrode surfaces were subsequently characterized. The electrochemical nitrate reduction was studied under both constant current density and constant potential conditions, comparing the performance of Cu/Ni and PdCu/Ni electrodes. Additionally, the nitrate reduction reaction on Cu10min/Ni was investigated using the electrochlorination process to examine $N_2$ evolution and chlorine species. The conclusions of this research are summarized below

.

## 5.1 Conclusions

1. By increasing the plating time, the plated Cu on Ni foam demonstrated a higher ratio of Cu(200)/Cu(111) and an improved electron transfer ability. Pd plated on Cu10min/Ni exhibited an even better electron transfer ability.
2. Electrochemical nitrate reduction using the prepared monometallic Cu and bimetallic PdCu electrodes on Ni foam showed high nitrate removal efficiency under a constant current density. 100% conversion of nitrate to $NH_4^+$ was achieved by Cu90min/Ni and PdCu10min/Ni in 210 and 180 minutes, respectively.



doi:10.6342/NTU202303029

3. The nitrate reduction reaction on Cu10min/Ni could be performed at a potential as low as $-0.6\text{V vs SCE}$. In acidic conditions, $NO_3^-$ was completely converted to $NH_4^+$ and no other products was generated for various applied constant potentials.
4. Under acidic conditions, neither different electrode properties nor controlled voltage could initiate nitrogen evolution. The dominant product observed was $NH_4^+$ in all experiments.
5. Addition of $Cl^-$ accelerated nitrogen evolution due to breakpoint chlorination. Small amounts of free chlorine and combined chlorine were detected.

## 5.2 Recommendations

1. The pH value of the solution may play a crucial role in $N_2$ generation due to the presence of hydrogen ions ($H^+$). The influences of pH on the formation of $N_2$ in electrochemical reduction of $NO_3^-$ should be investigated.
2. The bimetallic catalyst PdCu10min/Ni did not exhibit nitrate reduction activity under constant potential. Further study could focus on researching the selectivity of $N_2$ and $NH_3$ using different metals.



doi:10.6342/NTU202303029

3. To achieve the high nitrogen gas evolution, electrochlorination is evitable while the residual $Cl^-$ can affect the environmental and human health. In other to reduce this effect, chlorine gas evolution on anode should be studied by adjusting operation time and applying potential.



doi:10.6342/NTU202303029

# Reference


Speight, J. G. (2017). Industrial Inorganic Chemistry. In *Environmental Inorganic Chemistry for Engineers* (pp. 111-169). https://doi.org/10.1016/b978-0-12-849891-0.00003-5

Fewtrell, L. (2004). Drinking-Water Nitrate, Methemoglobinemia, and Global Burden of Disease: A Discussion. *Environmental Health Perspectives*, *112*(14), 1371-1374. https://doi.org/10.1289/ehp.7216

Hornung, M. (1999). The Role of Nitrates in the Eutrophication and Acidification of Surface Waters. *Managing Risks of Nitrates to Humans and the Environment*, 155-174. https://doi.org/10.1533/9781845693206.155

Atangana Njock, P. G., Zhou, A., Yin, Z., & Shen, S.-L. (2023). Integrated risk assessment approach for eutrophication in coastal waters: Case of Baltic Sea. *Journal of Cleaner Production, 387*. https://doi.org/10.1016/j.jclepro.2022.135673

International Comparison of Water Quality (2020). Retrieved from https://english.water.gov.taipei/cp.aspx?n=ED0C1E259A61491D&s=C17809EB5BA6F5E7

Taiwan Environmental Protection Administration (2022). Retrieved from https://oaout.epa.gov.tw/law/EngLawContent.aspx?lan=E&id=295&KW=nitrate

Min, B., Gao, Q., Yan, Z., Han, X., Hosmer, K., Campbell, A., & Zhu, H. (2021). Powering the Remediation of the Nitrogen Cycle: Progress and Perspectives of Electrochemical Nitrate Reduction. *Industrial & Engineering Chemistry Research*, *60*(41), 14635-14650. https://doi.org/10.1021/acs.iecr.1c03072




doi:10.6342/NTU202303029

SSINA (SPECIALTY STEEL INDUSTRY OF NORTH AMERICA) (2020). Retrieved from https://www.ssina.com/education/fabrication/passivation/

Hocking, M. B. (2005). Ammonia, Nitric Acid and Their Derivatives. *Handbook of Chemical Technology and Pollution Control (Third Edition)*, 321-364. https://doi.org/10.1016/B978-012088796-5/50014-4

Manisalidis, I., Stavropoulou, E., Stavropoulos, A., & Bezirtzoglou, E. (2020). Environmental and Health Impacts of Air Pollution: A Review. *Frontiers in Public Health*, *8*. https://doi.org/10.3389/fpubh.2020.00014

Moloantoa, K. M., Khetsha, Z. P., van Heerden, E., Castillo, J. C., & Cason, E. D. (2022). Nitrate Water Contamination from Industrial Activities and Complete Denitrification as a Remediation Option. *Water*, *14*(5), 799. https://doi.org/10.3390/w14050799

Kurt, E., Koseoglu-Imer, D. Y., Dizge, N., Chellam, S., & Koyuncu, I. (2012). Pilot-scale evaluation of nanofiltration and reverse osmosis for process reuse of segregated textile dye wash wastewater. *Desalination*, *302*, 24-32. https://doi.org/10.1016/j.desal.2012.05.019

Shelly, Y., Kuk, M., Menashe, O., Zeira, G., Azerrad, S., & Kurzbaum, E. (2021). Nitrate removal from a nitrate-rich reverse osmosis concentrate: Superior efficiency using the bioaugmentation of an Acinetobacter biofilm. *Journal of Water Process Engineering*, *44*, 102425. https://doi.org/10.1016/j.jwpe.2021.102425

Zhang, J., Fan, C., Zhao, M., Wang, Z., Jiang, S., Jin, Z., Bei, K., Zheng, X., Wu, S., Lin, P., & Miu, H. (2023). A comprehensive review on mixotrophic denitrification processes for biological nitrogen removal. *Chemosphere*, *313*, 137474.



doi:10.6342/NTU202303029

https://doi.org/10.1016/j.chemosphere.2022.137474

Giddey, S., Badwal, S. P. S., Munnings, C., & Dolan, M. (2017). Ammonia as a Renewable Energy Transportation Media. *ACS Sustainable Chemistry & Engineering*, *5*(11), 10231-10239. https://doi.org/10.1021/acssuschemeng.7b02219

Jin, H., Guo, C., Liu, X., Liu, J., Vasileff, A., Jiao, Y., Zheng, Y., & Qiao, S. Z. (2018). Emerging Two-Dimensional Nanomaterials for Electrocatalysis. *Chem Rev*, *118*(13), 6337-6408. https://doi.org/10.1021/acs.chemrev.7b00689

Shih, Y.-J., Wu, Z.-L., Lin, C.-Y., Huang, Y.-H., & Huang, C.-P. (2020). Manipulating the crystalline morphology and facet orientation of copper and copper-palladium nanocatalysts supported on stainless steel mesh with the aid of cationic surfactant to improve the electrochemical reduction of nitrate and N2 selectivity. *Applied Catalysis B: Environmental*, *273*. https://doi.org/10.1016/j.apcatb.2020.119053

Shih, Y.-J., Wu, Z.-L., Huang, Y.-H., & Huang, C.-P. (2020). Electrochemical nitrate reduction as affected by the crystal morphology and facet of copper nanoparticles supported on nickel foam electrodes (Cu/Ni). *Chemical Engineering Journal*, *383*. https://doi.org/10.1016/j.cej.2019.123157

Zhang, X., Wang, Y., Liu, C., Yu, Y., Lu, S., & Zhang, B. (2021). Recent advances in non-noble metal electrocatalysts for nitrate reduction. *Chemical Engineering Journal*, *403*, 126269. https://doi.org/10.1016/j.cej.2020.126269

Su, J. F., Kuan, W.-F., Chen, C.-L., & Huang, C.-P. (2020). Enhancing electrochemical nitrate reduction toward dinitrogen selectivity on Sn-Pd bimetallic electrodes by surface structure design. *Applied Catalysis A: General*, *606*.



doi:10.6342/NTU202303029

https://doi.org/10.1016/j.apcata.2020.117809

Cao, Y., Yuan, S., Meng, L., Wang, Y., Hai, Y., Su, S., Ding, W., Liu, Z., Li, X., & Luo, M. (2023). Recent Advances in Electrocatalytic Nitrate Reduction to Ammonia: Mechanism Insight and Catalyst Design. *ACS Sustainable Chemistry & Engineering*, *11*(21), 7965-7985. https://doi.org/10.1021/acssuschemeng.3c01084

Ai, F., & Wang, J. (2022). Theoretical Evaluation of Electrochemical Nitrate Reduction Reaction on Graphdiyne-Supported Transition Metal Single-Atom Catalysts. *ACS Omega*, *7*(35), 31309-31317. https://doi.org/10.1021/acsomega.2c03588

Teng, M., Ye, J., Wan, C., He, G., & Chen, H. (2022). Research Progress on Cu-Based Catalysts for Electrochemical Nitrate Reduction Reaction to Ammonia. *Industrial & Engineering Chemistry Research*, *61*(40), 14731-14746. https://doi.org/10.1021/acs.iecr.2c02495

Duca, M., Koper, M., (2012). Powering denitrification: the perspectives of electrocatalytic nitrate reduction. *Energy Environ. Sci.*, 2012,5**,** 9726-9742

https://doi.org/10.1039/C2EE23062C

Lu, X., Song, H., Cai, J., & Lu, S. (2021). Recent development of electrochemical nitrate reduction to ammonia: A mini review. *Electrochemistry Communications*, *129*. https://doi.org/10.1016/j.elecom.2021.107094

Wu, Z.-L., & Shih, Y.-J. (2022). Bimetallic palladium-tin nanoclusters, PdSn(2 0 0) and PdSn(1 0 1), templated with cationic surfactant for electrochemical denitrification toward $N_2$ and $NH_4^+$ selectivity. *Chemical Engineering Journal*, *433*. https://doi.org/10.1016/j.cej.2021.133852



doi:10.6342/NTU202303029

Shin, H., Jung, S., Bae, S., Lee, W., & Kim, H. (2014). Nitrite reduction mechanism on a Pd surface. *Environ Sci Technol*, *48*(21), 12768-12774. https://doi.org/10.1021/es503772x

Ebbesen, S. D., Mojet, B. L., & Lefferts, L. (2010). Effect of PH on the Nitrite Hydrogenation Mechanism over $Pd/Al_2O_3$ and $Pt/Al_2O_3$: Details Obtained with ATR-IR Spectroscopy. *J. Phys. Chem. C* **2011,** *115*, 1186–1194. https://doi.org/10.1021/jp106521t

Cerrón-Calle, G. A., Fajardo, A. S., Sánchez-Sánchez, C. M., & Garcia-Segura, S. (2022). Highly reactive Cu-Pt bimetallic 3D-electrocatalyst for selective nitrate reduction to ammonia. *Applied Catalysis B: Environmental*, *302*. https://doi.org/10.1016/j.apcatb.2021.120844

Li, L., Yun, Y., Zhang, Y., Huang, Y., & Xu, Z. (2018). Electrolytic reduction of nitrate on copper and its binary composite electrodes. *Journal of Alloys and Compounds*, *766*, 157-160. https://doi.org/10.1016/j.jallcom.2018.07.004

Shen, Z., Liu, D., Peng, G., Ma, Y., Li, J., Shi, J., Peng, J., & Ding, L. (2020). Electrocatalytic reduction of nitrate in water using Cu/Pd modified Ni foam cathode: High nitrate removal efficiency and $N_2$-selectivity. *Separation and Purification Technology*, *241*. https://doi.org/10.1016/j.seppur.2020.116743

Zhang, Y., Zhao, Y., Chen, Z., Wang, L., Wu, P., & Wang, F. (2018). Electrochemical reduction of nitrate via Cu/Ni composite cathode paired with Ir-Ru/Ti anode: High efficiency and $N_2$ selectivity. *Electrochimica Acta*, *291*, 151-160. https://doi.org/10.1016/j.electacta.2018.08.154

Favarini Beltrame, T., Gomes, M. C., Marder, L., Marchesini, F. A., Ulla, M. A., & Moura Bernardes, A. (2020). Use of copper plate electrode and Pd catalyst to the



doi:10.6342/NTU202303029

nitrate reduction in an electrochemical dual-chamber cell. *Journal of Water Process Engineering*, *35*, 101189. https://doi.org/10.1016/j.jwpe.2020.101189

Li, J., Gao, J., Feng, T., Zhang, H., Liu, D., Zhang, C., Huang, S., Wang, C., Du, F., Li, C., & Guo, C. (2021). Effect of supporting matrixes on performance of copper catalysts in electrochemical nitrate reduction to ammonia. *Journal of Power Sources*, *511*. https://doi.org/10.1016/j.jpowsour.2021.230463

Wang, S., Lu, A., & Zhong, C. J. (2021). Hydrogen production from water electrolysis: role of catalysts. *Nano Converg*, *8*(1), 4. https://doi.org/10.1186/s40580-021-00254-x

Garcia-Segura, S., Lanzarini-Lopes, M., Hristovski, K., & Westerhoff, P. (2018). Electrocatalytic reduction of nitrate: Fundamentals to full-scale water treatment applications. *Applied Catalysis B: Environmental*, *236*, 546-568. https://doi.org/10.1016/j.apcatb.2018.05.041

Tan, X., Wang, X., Zhou, T., Chen, T., Liu, Y., Ma, C., Guo, H., & Li, B. (2022). Preparation of three dimensional bimetallic Cu-Ni/NiF electrodes for efficient electrochemical removal of nitrate nitrogen. *Chemosphere*, *295*, 133929. https://doi.org/10.1016/j.chemosphere.2022.133929

Liu, G., Yu, J. C., Lu, G. Q., & Cheng, H. M. (2011). Crystal facet engineering of semiconductor photocatalysts: motivations, advances and unique properties. *Chem Commun (Camb)*, *47*(24), 6763-6783. https://doi.org/10.1039/c1cc10665a

Lee, J. M., Jung, K. K., & Ko, J. S. (2016). Growth Mechanism and Application of Nanostructures Fabricated by a Copper Sulfate Solution Containing Boric Acid. *Journal of The Electrochemical Society*, *163*(8), D407-D413. https://doi.org/10.1149/2.0691608jes



doi:10.6342/NTU202303029

Islam, M. N., & Channon, R. B. (2020). Electrochemical sensors. In *Bioengineering Innovative Solutions for Cancer* (pp. 47-71). https://doi.org/10.1016/b978-0-12-813886-1.00004-8

Sun, D., Monaghan, P., Brantley, W. A., & Johnston, W. M. (2002). Electrochemical impedance spectroscopy study of high-palladium dental alloys. Part I: behavior at open-circuit potential. *J Mater Sci Mater Med*, *13*(5), 435-442. https://doi.org/10.1023/a:1014719513624

Du, C., Shang, M., Mao, J., & Song, W. (2017). Hierarchical MoP/Ni2P heterostructures on nickel foam for efficient water splitting. *Journal of Materials Chemistry A*, *5*(30), 15940-15949. https://doi.org/10.1039/c7ta03669h

Wei, C., Sun, S., Mandler, D., Wang, X., Qiao, S. Z., & Xu, Z. J. (2019). Approaches for measuring the surface areas of metal oxide electrocatalysts for determining their intrinsic electrocatalytic activity. *Chem Soc Rev*, *48*(9), 2518-2534. https://doi.org/10.1039/c8cs00848e

Connor, P., Schuch, J., Kaiser, B., & Jaegermann, W. (2020). The Determination of Electrochemical Active Surface Area and Specific Capacity Revisited for the System MnOx as an Oxygen Evolution Catalyst. *Zeitschrift für Physikalische Chemie*, *234*(5), 979-994. https://doi.org/10.1515/zpch-2019-1514

Masa, J., Andronescu, C., & Schuhmann, W. (2020). Electrocatalysis as the Nexus for Sustainable Renewable Energy: The Gordian Knot of Activity, Stability, and Selectivity. *Angew Chem Int Ed Engl*, *59*(36), 15298-15312. https://doi.org/10.1002/anie.202007672

Elgrishi, N., Rountree, K. J., McCarthy, B. D., Rountree, E. S., Eisenhart, T. T., & Dempsey, J. L. (2017). A Practical Beginner's Guide to Cyclic Voltammetry.



doi:10.6342/NTU202303029

*Journal of Chemical Education*, *95*(2), 197-206. https://doi.org/10.1021/acs.jchemed.7b00361

Wada, K., Hirata, T., Hosokawa, S., Iwamoto, S., & Inoue, M. (2012). Effect of supports on Pd–Cu bimetallic catalysts for nitrate and nitrite reduction in water. *Catalysis Today*, *185*(1), 81-87. https://doi.org/10.1016/j.cattod.2011.07.021

Iwamoto, M., Akiyama, M., Aihara, K., & Deguchi, T. (2017). Ammonia Synthesis on Wool-Like Au, Pt, Pd, Ag, or Cu Electrode Catalysts in Nonthermal Atmospheric-Pressure Plasma of N2 and H2. *ACS Catalysis*, *7*(10), 6924-6929. https://doi.org/10.1021/acscatal.7b01624

Dima, G. E., de Vooys, A. C. A., & Koper, M. T. M. (2003). Electrocatalytic reduction of nitrate at low concentration on coinage and transition-metal electrodes in acid solutions. *Journal of Electroanalytical Chemistry*, *554-555*, 15-23. https://doi.org/10.1016/s0022-0728(02)01443-2

Duncan, H., & Lasia, A. (2008). Separation of hydrogen adsorption and absorption on Pd thin films. *Electrochimica Acta*, *53*(23), 6845-6850. https://doi.org/10.1016/j.electacta.2007.12.012

Sun, W., Li, Q., Gao, S., & Shang, J. K. (2012). Monometallic Pd/Fe3O4 catalyst for denitrification of water. *Applied Catalysis B: Environmental*, *125*, 1-9. https://doi.org/10.1016/j.apcatb.2012.05.014

Gombas, D., Luo, Y., Brennan, J., Shergill, G., Petran, R., Walsh, R., Hau, H., Khurana, K., Zomorodi, B., Rosen, J., Varley, R., & Deng, K. (2017). Guidelines To Validate Control of Cross-Contamination during Washing of Fresh-Cut Leafy Vegetables. *J Food Prot*, *80*(2), 312-330. https://doi.org/10.4315/0362-028X.JFP-16-258



doi:10.6342/NTU202303029

Mostafa, E., Reinsberg, P., Garcia-Segura, S., & Baltruschat, H. (2018). Chlorine species evolution during electrochlorination on boron-doped diamond anodes: In-situ electrogeneration of Cl2, Cl2O and ClO2. *Electrochimica Acta*, *281*, 831-840. https://doi.org/10.1016/j.electacta.2018.05.099

Ordeig, O., Mas, R., Gonzalo, J., Del Campo, F. J., Muñoz, F. J., & de Haro, C. (2005). Continuous Detection of Hypochlorous Acid/Hypochlorite for Water Quality Monitoring and Control. *Electroanalysis*, *17*(18), 1641-1648. https://doi.org/10.1002/elan.200403194



doi:10.6342/NTU202303029